ADVANCED OPTICAL MATERIALS
www.advopticalmat.de

Progress Toward Stable Organic Solar Cells

*Newayemedhin A. Tegegne, Leonato T. Nchinda, and Tjaart P. J. Krüger**

Organic solar cells (OSCs) are suitable candidates for next-generation renewable energy sources due to their low cost of production and flexibility. Their power conversion efficiency has improved significantly to about 20% in both single- and multi-junction devices due to the tremendous work in optimizing the synthesis of novel active-layer materials while improving device fabrication. Despite a few reports predicting a 20-year lifetime for OSC devices, their stability currently lags behind their commercialization. This Review discusses the issues that impair OSC stability and how to mitigate them. While emphasizing the importance of the International Summit on Organic Photovoltaic Stability (ISOS) protocols, an overview of recent advancements in OSC power conversion efficiency (PCE) and lifetime is provided. Finally, fundamental challenges to developing high-performance and stable OSCs are discussed along with general recommendations for improving the stability of OSCs.

1. Introduction

Organic solar cells (OSCs) provide a unique opportunity for a cost-efficient energy-generation technology due to their solution processability and mechanical flexibility, enabling mass production with simple roll-to-roll techniques. Their main advantages are, in particular, their use of abundant, non-toxic raw organic semiconductor materials that can be tailored to specific applications and the use of manufacturing technologies—primarily solution processing—that are capable of coating large areas inexpensively and fast.[1–3] This, combined with little material consumption (~1 g organic semiconductor per m^2), low-temperature processing, and compatibility with flexible substrates, enable lightweight devices made in roll-to-roll production and a large versatility in applications. Based on these properties, OSCs may become the world's cheapest source of energy. Concerted research has also witnessed a considerable improvement in the power conversion efficiency (PCE) of OSCs, regularly exceeding the milestone of 10%.[4–7] The champion devices with PCEs approaching and even exceeding 20% in single-junction devices[8–13] and over 20%[14] in tandem devices exceed the efficiency of commercial thin-film inorganic solar cells[15] and are close to the best-performing thin-film solar cells.[16] These advantages, together with the recorded high efficiencies, make OSCs the most advanced clean energy sources that are near commercialization.

The major impediment to the commercialization and widespread use of OSCs is their limited stability, evidenced by a considerable drop in efficiency over time. Degradation in OSCs can either be intrinsic, observed as spontaneous changes in the active layer, electrodes, or interfaces between the layers, or extrinsic, caused by light, water, oxygen, elevated temperatures, and/or mechanical stress.[17] The past ~two decades have witnessed an enormous effort to a deep understanding and mitigation of the degradation mechanisms in OSCs, which has led to a considerable improvement in their stability from a few minutes to a potential lifetime reaching over 10 years in the laboratory.[18] Structural engineering of donor (D) and acceptor (A) polymeric semiconductors to improve both their efficiency and stability has also been at the forefront of OSC research. Emphasis on their energy levels aimed at developing low band-gap materials to prevent oxidation has provided insight into degradation originating from the formation of reactive oxygen species (ROS). Another major research focus has been on the stabilization of the active-layer morphology, given that it is thermodynamically unstable and usually evolves to a more stable state over time. Techniques such as crosslinking, solvent additives, and the use of structurally stable D/A materials are among the strategies that have been employed to enhance the active-layer morphology, thereby improving the overall stability of OSC devices. The interfacial layers have also been an important research topic to enhance OSC stability as they directly influence the dynamics and collection of photogenerated charge carriers.[19–22]

N. A. Tegegne
Department of Physics
Addis Ababa University
Addis Ababa 1176, Ethiopia
L. T. Nchinda, T. P. J. Krüger
Department of Physics
University of Pretoria
Private Bag X20, Hatfield 0028, South Africa
E-mail: tjaart.kruger@up.ac.za
T. P. J. Krüger
National Institute for Theoretical and Computational Sciences (NITheCS)
South Africa

The ORCID identification number(s) for the author(s) of this article can be found under https://doi.org/10.1002/adom.202402257

© 2024 The Author(s). Advanced Optical Materials published by Wiley-VCH GmbH. This is an open access article under the terms of the Creative Commons Attribution-NonCommercial-NoDerivs License, which permits use and distribution in any medium, provided the original work is properly cited, the use is non-commercial and no modifications or adaptations are made.

DOI: 10.1002/adom.202402257

In this Review, recent developments in understanding the degradation of OSCs and strategies to limit their impact are summarized by focusing on each of the device layers. In Section 3, we explore the mechanisms that influence the stability of OSCs. The key reasons for reduced OSC lifetimes are highlighted as oxygen and water intrusion (Section 3.1.1), light exposure (Section 3.1.2), heating (Section 3.1.3), and unstable morphology of especially the active layer (Section 3.2). The importance of each OSC layer in the overall device degradation and various strategies to enhance each layer's stability are examined in Section 4. For easy comparability of results from different research laboratories, the ISOS protocols are described in Section 5.1, while highlighting the recent progress made in improving the PCE and lifetime of OSCs (Section 5.2). Finally, some fundamental challenges and prospects toward OSC commercialization are proposed in Section 6.

2. Working Principle of OSCs

OSCs are photovoltaic (PV) devices in which π-conjugated electron-donating and electron-accepting materials are sandwiched between two electrodes of opposite polarity. These conjugated polymers are characterized by alternating single and double bonds in their molecular structure, creating an extended π-conjugated system. This extended conjugation allows for a significant overlap of molecular orbitals along the polymer chain, enhancing the probability of electronic transitions and, consequently, the oscillator strength, which is directly related to the absorption efficiency. The absorption spectra of conjugated polymers are characterized by intense and broad bands. Their high absorption intensity can be attributed to extended π-conjugation, while their broad bandwidths result from their molecular heterogeneity, structural disorder, and the multitude of available vibronic transitions. These optical properties make π-conjugated polymers versatile materials for applications in optoelectronic devices, where their absorption characteristics are crucial for efficient light absorption and emission. A further increase in the absorption of OSC active layers can be realized by using non-fullerene acceptors (NFAs) instead of the commonly used fullerene acceptors, the inclusion of a third component, stacking of polymers with different optical band gaps in a tandem cell, and the use of plasmonic nanoparticles.[23,24]

2.1. Charge Generation and Transport

Photon absorption by an OSC results in the creation of a tightly bound electron-hole pair commonly known as an exciton with a binding energy of about 0.2–1 eV.[25] Once the neutral exciton is generated, it has to diffuse to the D/A interface to dissociate into positive and negative charge carriers. The D/A interface should thus be within the diffusion length of the exciton, which is typically below 20 nm. The availability of a D/A interface within the exciton diffusion length inspired the bulk heterojunction (BHJ) concept, a recommended alternative to the bilayer device structure that comprises a layer of donor material on top of an acceptor material. In a bilayer device, only excitons created 10–20 nm below the D/A contact (i.e., within the exciton diffusion length) have a high probability of dissociating into free charges. This limitation significantly hampers the efficiency of charge photogeneration. In contrast, a BHJ is characterized by an interpenetrating network of donor and acceptor domains, which allows a considerable enhancement in exciton dissociation due to the greatly increased D/A interfacial area within the photoactive layer.

The process of charge photogeneration following photon absorption in these devices resembles that of natural photosynthetic systems that convert sunlight into electron-hole pairs in the photochemical reaction centers. The four major steps of charge photogeneration in OSCs are exciton generation, exciton migration to a D/A interface, free charge generation across the interface, and charge transport. This is subsequently followed by charge collection by the electrodes to generate electricity. The PCE of OSCs depends on the efficiency of each of these processes. The long-term stability of OSCs can therefore be greatly improved if each of the processes is unaffected by external and internal stresses.

Free charge generation at the D/A interface involves multiple steps, as depicted in **Figure 1**. The first step involves partial dissociation of the exciton, forming a so-called charge-transfer (CT) state across the interface, which comprises a partial donor cation (D^+) and a partial acceptor anion (A^-) that are strongly Coulombically bound. The CT state can be considered a mixture between a pure excitonic and a fully charge-separated (CS) state, where in the former case (i.e., the exciton), the electron and hole are in the same donor molecule, while in the latter case (i.e., the CS state), the hole still resides in the highest occupied molecular orbital (HOMO) of the donor but the electron occupies the lowest unoccupied molecular orbital (LUMO) of the acceptor, i.e., an electron is fully transferred. The relaxed CT state typically has lower energy than the preceding singlet exciton state; hence, an isoenergetic transition to the CT state populates higher vibrational levels, known as a hot CT state (CT*). If full charge separation occurs immediately, i.e., before thermalization of the CT state, a hot charge-separated state (CS*) is populated. Charge separation may also occur from the lowest CT state after thermalization before or after intersystem crossing (ISC). These processes compete with geminate recombination from the singlet (^{1}CT) or triplet (^{3}CT) states. Ideally, the CS* state migrates away from the D/A interface while it relaxes thermally, consequently separating the charge carriers. If they do not leave the interface, a CT state may again be formed across the interface, populating the lowest CT state, from where geminate recombination may occur. There is also a possibility that the free charges may decay by bimolecular recombination while transported through the corresponding materials (the electrons in the acceptor, and the hole in the donor). If this does not happen before they are collected by the electrodes, an external circuit is formed, thus generating electricity. The completely unbound electron-hole pairs have an energy that is equivalent to the sum of the ionization potential of the donor and the electron affinity of the acceptor.

In contrast to conventional inorganic crystalline semiconductors, the morphology of OSC materials is more disordered and generally amorphous. Thus, instead of band transport, charge transport happens by "hopping" between the localized states within the active layer.[27] During this process, traps in the active layer—likely caused by defects, phase discontinuity, morphological disorder, and so forth—may prevent charges from reaching

© 2024 The Author(s). Advanced Optical Materials published by Wiley-VCH GmbH

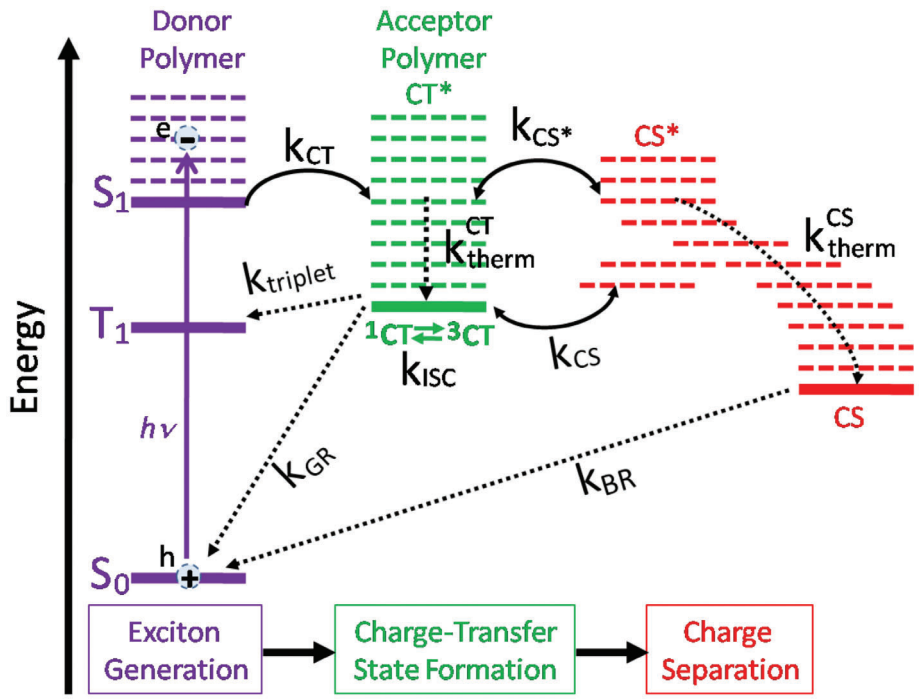

Figure 1. Main processes involved in charge photogeneration, shown in a qualitative electronic-state diagram. S_0 represents the donor's singlet ground state (i.e., HOMO), while S_1 represents the first singlet excited state (excitonic state, i.e., LUMO). Intermolecular charge transfer (CT) at the D/A interface generates CT states, where the D molecules have a hole and the A molecules have an electron. ^{1}CT and ^{3}CT represent, respectively, the lowest singlet and triplet CT states, while CT* and CS* denote excited ("hot") levels of the CT and charge-separated (CS) manifolds, respectively. The final state is the lowest-energy CS state, in which the holes and electrons have been completely separated. The k_i terms denote competing relaxation and electron-transfer rates. hv: Photoexcitation to singlet exciton (S_1). k^{CT}: Exciton dissociation to form the hot charge-transfer (CT) state. k^{CT}_{therm}: Thermal relaxation of the CT state. k_{ISC}: Spin mixing of the ^{1}CT and ^{3}CT states. $k_{triplet}$: Geminate recombination of the ^{3}CT to the triplet exciton, T_1. k_{GR}: Geminate recombination of the ^{1}CT state back to the ground state, S_0. k_{CS^*}: Dissociation of the hot CT state into a fully charge-separated (CS) state. k_{CS}: Dissociation of the thermally relaxed CT state into the CS state. k^{CS}_{therm}: Thermal relaxation of the CS state and migration away from the D/A interface, resulting in an increase in state degeneracy (entropy) and charge localization on lower energy sites (traps, etc.). k_{BR}: Bimolecular recombination of the CS state. Adapted with permission.[26] Copyright 2009, American Chemical Society.

the electrodes and instead force them to recombine. Non-geminate recombination—the recombination of an electron and a hole from separate excitons—can also result from surface traps, improper contact between the active layer and electrodes, or even the extraction of a counterion charge carrier by a corresponding electrode.

Charge carrier mobility is also an important parameter in determining the efficiency of charge carrier transport. Organic semiconductors have low charge carrier mobilities—typically in the range of $10^{-4} - 10^{-5}$ cm^2 V^{-1} s^{-1}. The active layer is therefore kept thin (~100 nm) to allow carriers to reach electrodes within their lifetime. Balancing charge mobilities is crucial to avoid significant space-charge effects, which occur when the mobility values of holes and electrons differ by 2 to 3 orders of magnitude, thus hampering charge extraction.[28] Surface recombination and interface dipoles can also cause a "double-dipoles" phenomenon, further limiting charge extraction.[29,30]

2.2. Device Structure of OSCs

The device architecture of OSCs determines the charge collection paths. In the normal (traditional) geometry, the holes are collected by the high-work-function (WF) electrode, while the polarity is the opposite in the inverted geometry (see **Figure 2**). High-WF transparent oxides such as indium tin oxide (ITO) are coated with a hole-transport layer (HTL) in the traditional geometry, allowing hole collection by the electrode, while an electron-transport layer (ETL) such as zinc oxide (ZnO) is deposited on top of ITO in the inverted geometry, as shown in Figure 2. The HTLs and ETLs are deposited in the traditional and inverted geometry, respectively, before the deposition of the top electrode (e.g., Al, Ag) to cap the device. In both structures, the active layer is sandwiched between the transparent ITO electrode and the top metal electrode (e.g., Al, Ag). However, due to the energy mismatch between the electrodes and the active layer, charge extraction and recombination may be impeded and the charge-separated free carriers tend to recombine at the active layer/electrode interfaces when there is no selectivity for charge collection.[31] These issues are commonly addressed by adding interface layers between the active layer and electrodes to suppress charge recombination. To this end, ETLs are used to help transport electrons while blocking holes, and HTLs do the opposite: transport holes and stop electrons. The insertion of ETLs and HTLs also forms Ohmic contacts at the interfaces, reducing energy barriers for charge transport and tuning the different polarities of OSCs, which contribute to enhanced efficiencies.

© 2024 The Author(s). Advanced Optical Materials published by Wiley-VCH GmbH

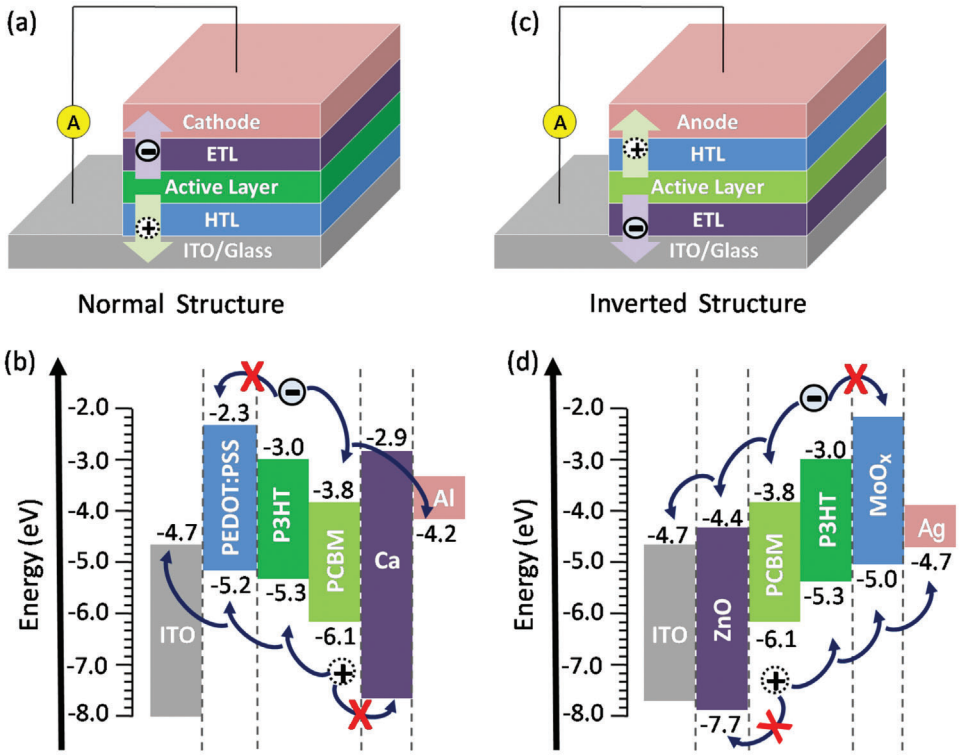

Figure 2. Schematic representations and band energy diagrams for the normal ((a) and (b), respectively) and inverted ((c) and (d), respectively) configurations of OSCs.

In the standard or normal ITO/HTL/active layer/ETL/metal structure, ITO serves as the anode, and a low-WF metal (e.g., Al or Ca) on top of the device serves as the cathode. For example, in the case of the well-known blend of poly(3-hexylthiophene-2,5-diyl) and [6,6]-phenyl-C71 butyric acid methyl ester (P3HT:$PC_{71}BM$) as the active layer, electrons are transported from P3HT to PCBM, which are selectively transported by the ETL and collected by the cathode. On the other hand, holes are left in P3HT domains and selectively transported by the poly(styrene sulfonic acid)-doped poly(3,4-ethylenedioxythiophene) (PEDOT:PSS) HTL and extracted by the ITO anode. This structure, however, has intrinsic device instability concerns. The low-WF metals deposited on top are particularly sensitive to oxygen and moisture, rendering them easily oxidized and corroded, thus exposing the active layers to rapid degradation in air.[32,33] Furthermore, PEDOT:PSS is commonly employed as the HTL, with benefits such as transparency, solution processing, and high conductivity.[34,35] However, the high acidic and hygroscopic nature of PSS can eventually compromise device performance by etching the ITO at the bottom over time.[36] Additionally, in the presence of external stress, such as high temperatures of about 65 °C, fullerenes and donor polymers aggregate, and the adhesion of polymers to the upper electrode creates a barrier to electron extraction, as reported by Sachs–Quintana et al., after they observed a recovery in efficiency upon peeling off the aged electrode and re-evaporating a new one.[31] To avoid this degradation phenomenon in the normal structure, an inverted structure is employed, where holes are extracted from the upper electrode.

Looking at the inverted ITO/ETL/active layer/HTL/metal structure, ITO acts as the cathode and the top metal (e.g., Ag or Au) as an anode, determined by the selectivity of the electron- and hole-transport layers. In the P3HT:$PC_{71}BM$ model system, electrons are transferred from P3HT to $PC_{71}BM$, transported via the ETL (e.g., ZnO), and extracted by the bottom ITO cathode, while the HTL (e.g., MoO_x) selectively transports the holes left in P3HT domains to the top anode for charge collection. Generally, solution-processable ETLs like ZnO, TiO_2, and SnO_2 are used to reduce the energy barrier, while HTLs such as MoO_x and WO_3 are deposited on the active layer.[31,37] Alternatives that can be used as interface layers, such as conjugated or non-conjugated organic materials like PFN and PEIE, can also contribute to large efficiencies in OSC devices. Nonetheless, when looking at stability issues critical for OSC commercialization, metal oxides with higher operational stability are preferred for practical applications. In contrast to the normal structure, the inverted configuration eliminates the need for PEDOT:PSS at the ITO surface while using an air-stable high-WF metal as the top anode. This effectively alleviates the degradation issue of the top electrode. Although there is no significant difference in efficiency between normal and inverted structures, a careful review of OSC stability suggests that an inverted architecture is the better option for future OSC applications.

3. OSC Degradation Factors and Mechanisms

The overall degradation of OSCs is determined by the degradation of each layer and their interfaces, where the main

© 2024 The Author(s). Advanced Optical Materials published by Wiley-VCH GmbH

mechanism by which OSCs lose their operation lifetime may be different across devices. The degradation can be either extrinsic due to water and air ingress, irradiation, and mechanical stress, or intrinsic due to a thermodynamically unstable morphology and/or diffusion among the layers. Intrinsic factors are those that occur spontaneously, without external stimuli, and are principally driven by the materials' inherent features. Intrinsic degradation would thus be relevant for OSCs that are thermally isolated and kept in an inert atmosphere, free from mechanical stresses. This division between external and internal degradation factors does not imply mutually exclusive factors; instead, the different degradation mechanisms often promote one another or operate together. In this Section, we summarize recent progress in our understanding of the degradation mechanisms in OSCs.

3.1. Extrinsic Factors of Degradation

OSCs without encapsulation generally experience significant extrinsic degradation in an ambient atmosphere due to exposure to oxygen and water as well as mechanical stress. Light illumination expedites the degradation due to photochemical mechanisms, most of which involve oxidation, that can degrade each of the OSC layers. Encapsulated devices still experience thermal degradation resulting from ambient temperature fluctuations, where significant heating can arise from direct and indirect solar radiation (including sources such as electron–hole recombination).

3.1.1. Oxygen and Water Ingress

In unencapsulated OSC devices prepared and characterized under ambient conditions, oxygen and water penetrate deep into the OSC through defects. The water molecules permeating the device can penetrate the active layer, forming trap states that reduce the charge photogeneration in the device due to its low ionization energy.[38] In particular, water diffusion into the active layer leads to the formation of OH^- in the backbone structure of the polymers, giving rise to polymer swelling and movement. In most cases, active-layer materials are chemically unstable when in contact with water. Fullerene acceptors, specifically, are reported to undergo an irreversibly strong modification of their HOMO structure.[39] In sharp contrast, NFAs undergo minor reversible changes that leave their energy levels largely unaffected.[40]

Water intrusion is particularly facilitated when the hygroscopic PEDOT:PSS blend is employed as HTL. This leads to a change in its morphology and properties, such as shifting its work function toward the vacuum level, thus hampering charge extraction. Additionally, the Al electrode in the standard design may become oxidized as a result of water vapor diffusion via the PEDOT:PSS layer.[41] Furthermore, oxidation of the cathode after water ingress occurs frequently from the edges, resulting in a reduction in the active area and, consequently, in PCE. Water infiltration causes OSC degradation, which results in an S-shaped current–voltage (*I*–*V*) curve due to worsened charge extraction, finally destroying the device's performance. Another degradation mechanism caused by water infiltration is layer delamination, which includes the PEDOT:PSS/active-layer interfaces.[42] Furthermore, the active-layer area is reduced due to water penetration,[43] which oxidizes the top electrode predominantly through the reaction of water with the HTL/active-layer interface, ultimately reducing device performance.[44] Decreasing the wettability of PEDOT:PSS reduces its hygroscopic character, which prevents water diffusion in and out. Anionic perfluorinated ionomer (PFI) additives used in PEDOT:PSS were found to limit water intrusion, boosting both the efficiency and stability of the device.[45] Aside from the hygroscopic PEDOT:PSS, a recent study has found that a ZnO ETL is unstable in water, forming large polymer aggregates in the active layer as a result of its poor chemical stability in water.[46]

Oxygen penetration is another common extrinsic degradation factor known to considerably reduce the lifetime of OSCs. The main oxygen-induced degradation mechanisms are photooxidation of the active-layer materials (see Section 3.1.2) and oxidation of the low-WF electrodes, while elevated temperatures usually expedite the reactions. Oxidation of the low-WF electrodes results in the formation of metal-oxide layers with reduced conductivity. These (partially) insulating layers form charge extraction barriers between the metal electrodes and active layer.[47–49] As a result, oxygen and water can then infiltrate into the active layer and the entire device via the electrode pinholes or grain boundaries.

OSCs undergo oxidation even in the dark due to p-type doping of O_2 on polymer donors, resulting in excess mobile holes and the formation of a charge extraction barrier layer for electrons.[48,49] This process is reversible in vacuum or inert atmospheres and does not involve chemical oxidation of the materials. However, when exposed to both light and O_2, permanent absorption bleaching occurs due to the degradation of conjugated bonds and the loss of chromophores, as demonstrated by Fourier-transform infrared spectroscopy measurements.[50–52] This oxidation reaction starts with free radical diffusion and progresses to side-chain degradation, resulting in a considerable decrease in photon absorption (photobleaching) and a decrease in the short-circuit current density, J_{SC}. Increased recombination and trap density, and the formation of bandgap defects may also be observed.

Device encapsulation using glass or plastic layers is a common strategy to minimize oxygen and water ingress. Glass is an effective material to suppress water permeability because, although molecular water readily diffuses into glass, the water molecules react with the glass matrix to form immobile hydroxyl groups.[53] In the case of silica glass, the dissolved water molecules form SiOH groups inside the glass. In contrast, molecular oxygen does not readily react or interact with the glass matrix but diffuses through the glass, albeit at a relatively slow rate.[54] An additional, slower permeability component results from oxygen diffusion through vacancy and interstitial sites in the glass matrix.[54] Therefore, unlike water, oxygen degradation is difficult to control, even with the best encapsulation. Plastics are generally considerably less effective encapsulation materials as oxygen and water have a relatively high permeability through polymers.

Oxidation of the active layer can be reduced by increasing the thickness of the encapsulating layer (since oxygen diffusion through glass, in particular, is relatively slow), using more crystalline polymers with denser layers (as they are more resistant to oxidation), removing unstable side-chains that are easily oxidized, using acceptors with deeper LUMO levels, and adding getter materials to absorb unwanted O_2.[55] As for the electrodes and interface layers, the use of high-WF metals such as silver and gold

© 2024 The Author(s). Advanced Optical Materials published by Wiley-VCH GmbH

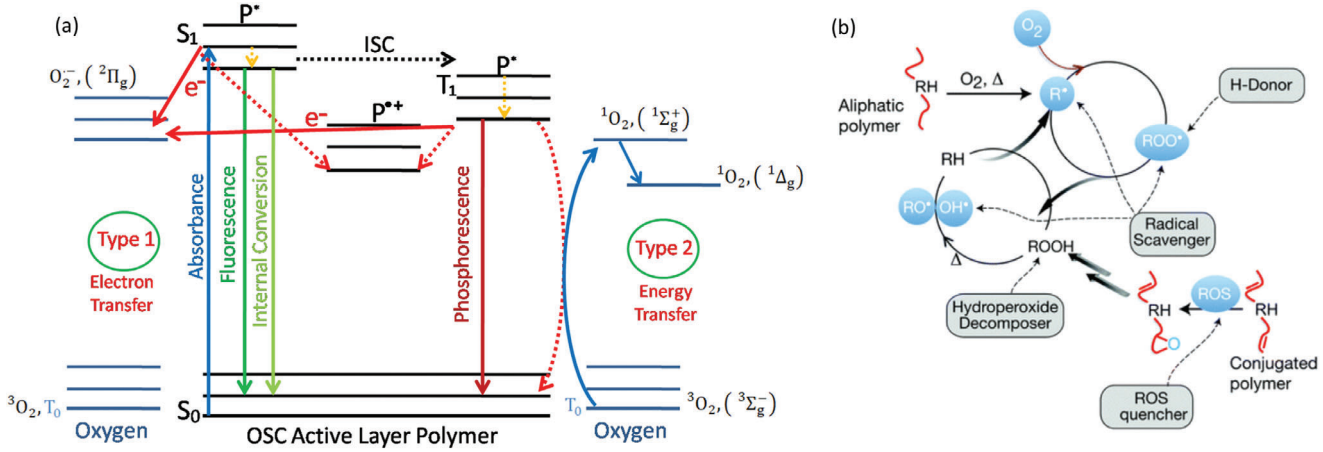

Figure 3. Main photooxidation mechanisms in OSCs. a) Primary photooxidation reactions in polymers—Type 1 and Type 2 reactions—between an active-layer polymer and molecular oxygen, shown in a Jablonski diagram. The Type 1 reaction (electron transfer) takes place either from the triplet state (T_1) or, less likely, from the singlet state (S_1, LUMO). Solid red arrows denote electron transfer, while dotted arrows represent transitions to the respective radical states. The Type 2 reaction (energy transfer to molecular oxygen) takes place from T_1. The main competing photophysical processes are represented by differently colored arrows. Yellow dotted arrows denote vibrational relaxation. ISC, intersystem crossing. b) Some secondary photooxidation mechanisms of polymers. See text for details. Reproduced with permission.[57] Copyright 2017, Royal Society of Chemistry.

instead of low-WF metals can help prevent deterioration as they are not easily oxidized. Also, increasing the thickness of the electrode and replacing PEDOT:PSS with hydrophobic materials can improve OSC protection and stability, respectively.[56]

3.1.2. Photodegradation

Generally, a fast initial PV performance loss is observed when most OSCs operate under light illumination, typically referred to as burn-in losses, and varies among materials.[58–60] Photooxidation of the photoactive layers is the most common degradation mechanism in OSCs. The photooxidation mechanisms have been well-established for macromolecular commodity polymers and are equally applicable to conjugated polymers. Both donor and acceptor materials can undergo photooxidation—conjugated polymers as well as molecules (like fullerene). The initial step of photooxidation of a light-sensitive polymer or molecule occurs through a direct reaction of the polymer or molecule in its excited state with molecular oxygen and proceeds through one of two pathways, called Type 1 and Type 2 reactions, as shown in **Figure 3a**. In both Type 1 and 2 reactions, the excited polymer or molecule acts as a photosensitizer. In the following, the mechanisms will be described for polymers but hold equally for molecules.

The Type 1 pathway occurs when an electron is transferred from the polymer to molecular oxygen to form a polymer cation ($P^{\bullet+}$) and a superoxide anion radical ($O_2^{\bullet-}$ or $O_2(^2\Pi_g)$). The Type 1 reaction is more likely to occur when the polymer is in a triplet state but electron transfer from the polymer singlet state can also take place. $O_2^{\bullet-}$, in particular, is reasonably reactive and can initiate radical reactions to produce more ROS. Specifically, $O_2^{\bullet-}$ can be reduced to form hydrogen peroxide (H_2O_2) or, in the presence of moisture, can be protonated to form the hydroperoxide radical $HO_2^{\bullet}$. These ROS can readily initiate chain reactions with the donor or acceptor materials, especially with radicals on the polymer chain, which usually involve further oxidation reactions, leading to the degradation of the organic components within the solar cell. Electron spin resonance (ESR) is a useful method to detect radical-mediated photodegradation in π-conjugated polymers.[61] To mitigate photooxidation, researchers often explore materials or strategies that can inhibit the photoinduced electron-transfer process or scavenge the superoxide ions or other ROS that are formed. In polymer:fullerene blends, the formation of $O_2^{\bullet-}$ is usually inhibited due to the low LUMO level of PCBM.

The Type 2 pathway is fundamentally different because it involves energy transfer instead of electron transfer. This pathway involves the transfer of the excitation energy from the polymer's excited triplet state (T_1) to molecular oxygen in its ground state, which is a triplet state ($^3O_2$ or $O_2(^3\Sigma_g^+)$), thereby exciting the oxygen to its $O_2(^1\Sigma_g^+)$ singlet state, which is very short-lived, and decays immediately to the lower singlet state $O_2(^1\Delta_g)$. Singlet oxygen is also a highly reactive species that can react with various components, leading to the degradation of the active layer and a decrease in the overall performance of the device. Degradation in polymer:fullerene blends is predominantly driven by the Type 2 pathway—triplet-induced singlet oxygen generation via the polymer[62] or the fullerene acceptor.[63,64] Once singlet oxygen is formed, it can initiate many reactions or be added to a polymer through a Diels–Alder cycloaddition reaction, creating an intermediate endoperoxide, which subsequently decomposes the polymer.[65]

The probability of Type 1 and 2 reactions is determined by their relative rates compared to the other decay processes of the electronic excited states. Specifically, ISC and electron transfer from S_1 (LUMO) compete with fluorescence and internal conversion, while electron and energy transfer to molecular oxygen from T_1 compete with phosphorescence and delayed fluorescence.

Photo-oxidative degradation of polymers usually starts with an initiating radical that forms through a Type 1 reaction or reaction of the polymer (P) with ROS, leading to a chain of further

© 2024 The Author(s). Advanced Optical Materials published by Wiley-VCH GmbH

oxidation reactions that decompose the polymer into smaller radicals. In most cases, the polymer side chains are targeted first before the degradation proceeds to the backbone structure.[66] Figure 3b considers one such carbon center (RH) in a polymer chain that degrades into a carbon-centered radical ($R^{\bullet}$) through oxidation. This radical readily reacts with molecular oxygen ($^3O_2$) to form a chain-initiating peroxyl radical ($ROO^{\bullet}$). Reduction of $ROO^{\bullet}$ forms hydroxyperoxide (ROOH) and usually additional radicals through the reaction $ROO^{\bullet} + RH \rightarrow ROOH + R^{\bullet}$. ROOH is very photolabile and easily decomposes into free radicals that can attack the polymer, for example, by abstracting hydrogen from another carbon center in the polymer. In a conjugated polymer, ROOH can be formed when a C═C bond is epoxidized through an ene-reaction with ROS—usually singlet oxygen ($^1O_2$) (Figure 3b, lower right).

The probability of primary and secondary photooxidation reactions can be significantly reduced by using antioxidants such as β-carotene, which readily react with radicals, singlet oxygen, or with the triplet states of the photosensitized polymers or molecules, thus deactivating singlet oxygen[67,68] or quenching the sensitizer's triplet state before energy or electron transfer to O_2 can occur.[57] Furthermore, stabilizers such as nickel chelate S6 were found to significantly suppress photooxidation.[69]

Photoinduced degradation can also occur in the absence of oxygen, where the high-energy radiation reaching the earth's surface (ultraviolet (UV), specifically UV-A, UV-B, and gamma rays) can break certain chemical bonds. This process is known as radiolytic degradation. For example, blue light can break C—N bonds, UV-A radiation can break C—N bonds as well as C—C, C—O, and C—H bonds, while all these bonds as well as O═O and O—H bonds can be ruptured by UV-B radiation. In addition, gamma radiation can ionize atoms by causing electron ejection. Subsequently, chain scission in the polymers due to the cleavage of, for example, C—C and C—O bonds results in the creation of free radicals that can further decompose the polymer. In P3HT, saturation of the aromatic rings by the alkyl side chains by light-induced degradation in the absence of oxygen was also found to decrease the conjugation length, leading to a loss in absorbance.[70]

Since light-induced degradation is different for each of the active-layer materials, the energy-level alignment between the donor and the acceptor materials changes, which leads to excess recombination. Additionally, it was discovered that oxygen doping in the presence of light significantly lowers OSC performance due to unbalanced CT as the hole mobility rises as a result of the p-doping.[71] Wang et al. reported that light soaking increases disorder that leads to the rapid formation of trapped polaron pairs that eventually destroys the charge generation in PM6:Y6-based OSCs.[72] Diiodooctane (DIO) is a widely used additive to control the aggregation effect of PCBM in the active layer, resulting in a much-improved morphology. However, this molecule undergoes photolysis in the presence of UV light, generating reactive iodine and an iodooctane radical that can react with the polymer backbone to produce HI, which aggressively attacks the polymer chain.[73]

Photochemical reactions can also lead to chemical structure evolution or chain breakage, decreasing the optical density of the active layer and its absorption capability. This evolution can be tracked, for example, by measuring in-situ ultraviolet–visible (UV–VIS) absorption under illumination and can involve the degradation of various materials over a large time range, from seconds to hours. Infrared (IR) spectroscopy has also been used to probe changes in chemical structure, such as the reduction of conjugated bonds and the appearance of new groups like carbonyl and ester bonds.[50–52,74]

3.1.3. Thermal Degradation

OSCs working under continuous irradiation are prone to thermally-induced degradation as the device temperature is raised above the ambient condition. Thermal effects can be significant because, according to the Arrhenius equation, reaction rates have an exponential temperature dependence but only an approximately linear dependence on oxygen and UV-light exposure.[75] The thermal properties of the materials, mainly their glass transition temperature (T_g), crystallization, and phase transition, play a crucial role in the thermal stability of the device. The main thermally-induced degradation mechanisms include diffusion of the electrodes, buffer layers, and/or active-layer materials, thus inevitably modifying the morphology of the active layer, which is detrimental to the charge generation process. The active-layer morphology of a device can evolve into a network that does not favor charge generation mainly due to the crystallization of the components and their miscibility following thermal degradation.[76,77] When the miscibility between donor and acceptor materials is low, especially at higher temperatures, the donor (or acceptor) tends to aggregate and form larger-size clusters or domains, which may surpass the exciton diffusion length or charge transport length.[60,78]

Amorphous materials usually have better thermal stability due to the reduced crystallinity in the active-layer morphology in devices.[76] Furthermore, T_g of polymers is a critical parameter that dictates their molecular organization during solidification, which is mainly controlled by the backbone geometry and their side chains. Photoactive materials heated above T_g become mobile, causing a rapid coarsening and growth of large-sized crystals.[21] Heating also creates pinholes in the active layer that negatively affect the charge carrier transport and collection.[79] Moreover, thermally-induced coarsening and creation of fibril structures lead to an increased roughness that disrupts the interpenetrating network,[77,79–81] and at times lead to delamination of the electrodes and/or interfacial layers.

The core idea of BHJ OSCs involves a well-mixed donor-acceptor percolation microstructure for efficient charge generation at interfaces and charge extraction near electrodes. On the other hand, large-size pure phases can boost geminate recombination and impede charge generation, as excitons may not reach D/A interfaces within their lifetime, resulting in severe initial degradation and potentially causing burn-in.[82–84] Moreover, thermal cyclic chemical reactions that include chain scission may also degrade the device. Thermo-oxidation of active-layer materials is another well-documented degradation mechanism in OSCs that causes chain scission and ring opening.[85,86] Exposure of the polymers to an elevated temperature leads to chain breakage. Thermal degradation of polymers is usually associated with chain scission followed by radical formation, which initiates the degradation until the final termination stage, in which two compounds

© 2024 The Author(s). Advanced Optical Materials published by Wiley-VCH GmbH

with unpaired electrons form an inactive product, similar to the photooxidation reactions depicted in Figure 3(b).

3.1.4. Mechanical Degradation

OSCs must be made with outstanding, stable mechanical resilience in order to ensure their use in flexible and wearable applications. The mechanical response to stress differs from polymer to polymer and is determined mainly by the intermolecular and surface forces in the devices. The adhesion between the substrate and the film determines the strain at which cracks appear in the device, a common measure of the mechanical stability of the device. Amorphous structures are more flexible and less brittle than crystalline structures, giving them better mechanical stability. However, the prerequisites for high PCE in OSCs, such as extreme crystallinity and long conjugation lengths, do not guarantee that the materials will be durable mechanically.

One of the mechanical degradation mechanisms is due to a weak D/A interface with reduced polymer entanglement and density, resulting in poor resistance against crack growth and phase separation between the two components, hence poor mechanical stability.[87] Hence, the mechanical robustness of the active-layer materials of OSCs should be carefully selected by the addition of freezing components[68] and proper defect engineering.[88] Furthermore, the formation of poor active-layer morphology due to crystallinity changes[89] when the polymer chains align themselves to the direction of the strain and change from face-on to edge-on stacking or vice versa are among the few degradation processes that are deleterious to the mechanical robustness of the device.[42] Moreover, the adhesion between each of the layers of an OSC is sensitive to mechanical deformation that leads to degradation. For instance, crack formation in the electrodes can lead to delamination, which will subsequently kill the device's performance. Ref. [90] provides a detailed overview of the mechanical robustness of OSCs and strategies for achieving mechanical stability.

3.2. Intrinsic Factors of Degradation

External degradation factors such as diffusion of water and oxygen into the device can be reduced by the use of proper encapsulation. In contrast, intrinsic degradation, which includes the evolution of undesirable chemical properties as well as molecular arrangements at the device interfaces and within the active layer, occurs even when the encapsulation is perfect.[91]

The active layer of an OSC is metastable due to material diffusion, which leads to undesirable phase separation. Several intrinsic limitations contribute to this instability, including the spin-coating process's dependence on the complex kinetics of donor and acceptor materials. Achieving a balance between pure phase and phase-separated domains often results in an intrinsically unstable morphology. During spin coating, the bulk heterojunction morphology of OSCs is kinetically frozen, remaining far from thermodynamic equilibrium.[92,93] Consequently, the morphology evolves toward its thermodynamically stable state, which often does not support efficient charge generation. Even encapsulated devices can suffer degradation over time, as topological changes due to phase separation worsen, leading to vertically separated components within the active layer. Despite the degradation linked to intrinsic morphological instability, certain devices such as those based on PM6:Y6 have shown only slight degradation after 30 days of storage in the dark.[94] Achieving thicker active layers (on the order of several hundred nm) is essential for OSC commercialization. However, optimizing the morphology in thick active layers is particularly challenging, as maintaining vertical phase separation becomes more difficult. Cai et al. reported a 300 nm thick polymer solar cell (PSC) based on a PM6 donor and BTP-eC9 and L8-BO-F acceptors. Through a sequential layer-by-layer deposition method, they achieved vertically optimized phase separation, which led to an increased exciton diffusion length and a PCE of 17.31%.[95] Polymers with good solubility and controlled molecular aggregation allow acceptors to permeate the polymer layer, thereby increasing the D/A interface and achieving optimized vertical phase separation.[96] The vertical phase distribution of the constituents can evolve into a more stable distribution. The vertical distribution of the components in the active layer of an OSC determines its charge transport and recombination characteristics, hence strongly influencing its PCE. The interaction parameter ξ between the polymer and the acceptor is an important parameter determining this vertical phase separation. Strong interaction between the active-layer materials tends to cause surface-directed phase segregation, while weak interaction counteracts this vertical phase separation. Many OSCs show an evolution of this vertical phase separation with time.[97]

In addition to the morphology of the active layer, another intrinsic instability arises from the diffusion of materials at the interfaces into the photoactive layer. This highlights the importance of controlling the thermodynamic instability of the transport layers and electrodes to ensure the overall stability of the device.[98]. For example, a PM6:N3 OSC with a stable active layer experienced instability due to the diffusion of atoms from the charge transport layers and electrodes into the active layer.[99] The authors recommended further investigation into the instability of these interfaces and electrodes to enhance device stability. It is worth noting that atom diffusion from the electrode and buffer layers can occur even in encapsulated devices kept in controlled environments. Such diffusion can alter the energy levels of the buffer layers and electrodes, leading to the formation of traps that promote charge recombination. Intrinsic chemical instability of the materials used in OSCs can also lead to degradation, including the chemical reaction between constituents. For instance, a well-documented intrinsic degradation in non-fullerene-based OSCs includes the photo-catalytic activity of ZnO toward the small molecule dye ITIC, which can result in the formation of reactive oxygen species that degrade the dye and ultimately reduce the solar cell's efficiency.[100]

4. Stability-Enhancement Strategies for OSCs

The enormous effort to improve the efficiency of OSCs has brought forth champion performances exceeding 20% both in single- and multi-junction solar cells.[101,102] However, the limited stability of these devices is still hindering their commercialization. In this Section, recently published reports on strategies aimed at limiting OSC degradation are reviewed. The degradation of OSCs is a complex process that can be caused by

© 2024 The Author(s). Advanced Optical Materials published by Wiley-VCH GmbH

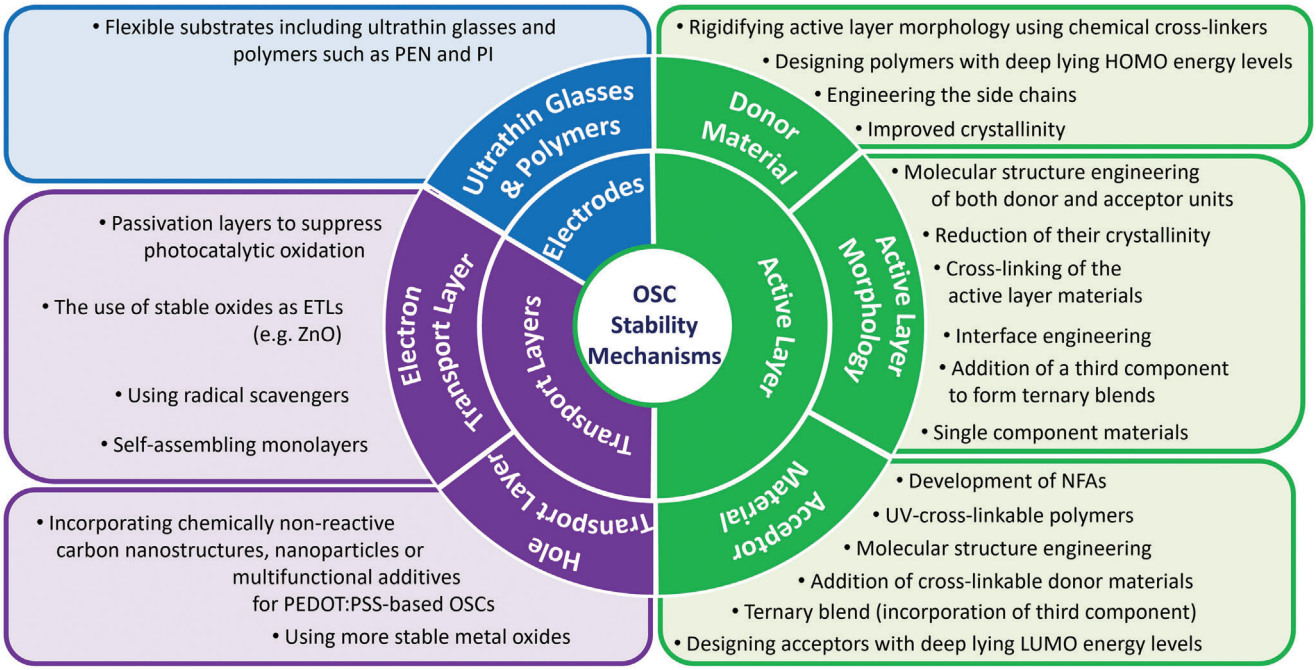

Figure 4. Commonly used strategies to improve OSC stability.

chemical degradation of the active-layer materials, the ETL and HTL, the electrodes, and/or the interfaces between each pair of layers. **Figure 4** gives a summary of the methods discussed in this Section that can be used to enhance the stability of OSC devices.

4.1. Active-Layer Stability

The active layer of OSCs is the absorber that plays the main role in charge generation, making its stability of paramount importance. The donor and acceptor materials in the active layer should be stable to ensure the stability of the device. Hence, a proper choice of these materials is crucial.

4.1.1. Acceptor Materials

Molecular structure modification of both the acceptors and donors has been reported to improve the stability of OSCs.[103–108] The long-employed buckyball fullerene acceptors have excellent electron mobility and high electron affinity.[109] However, these acceptors suffer from dimerization and aggregation[110,111] when exposed to external stressors such as light, which drastically reduces the PCE of fullerene-based solar cells. Some of the efforts to improve their stabilities include structural engineering[108,112] and the addition of crosslinkable donor materials to inhibit the aggregation of the fullerene acceptors.[106,113] The stability of P3HT:PCBM-based solar cells could be stabilized by adding 8% of poly(ethylene glycol) (PEG)-capped fullerene PCBM-PEG and [6,6]-phenyl-C61 butyric acid pentafluorophenyl ester ($PC_{61}BPF$).[114] Zhang et al. also reported the effectiveness of the recently employed novel fullerene derivative acceptors: a pyrrolidinofullerene (PyF5) and a methanofullerene (FAP1) (structures shown in **Figure 5**a), used in improving the thermal stability of devices, as the devices maintained over 93% of their initial PCE while the corresponding devices prepared with $PC_{60}BM$ maintained only 19%.[108] The authors attributed this exceptional stability to the better miscibility of the modified fullerene acceptors with the donor polymer PTB7-Th. UV-crosslinkable polymers based on PPDBT2FBT were found to inhibit the aggregation of $PC_{71}BM$ in the film, maintaining its morphology such that the PCE of the devices was sustained after 40 h of thermal stress at 120 °C.[106] The same study showed that this method additionally improved the photostability of the device. Polymerizable fullerene acrylates utilized in P3HT-based OSCs were also found to provide the device with significantly improved thermal stability while performing comparably to $PC_{71}BM$-based reference cells.[112] The best-performing acrylated fullerene-based device could retain 99.7% of its initial efficiency, whereas the reference device had only 11.8% remaining PCE after 35 h of heat treatment at 150 °C, owing to the polymerizable fullerenes becoming insoluble due to heating and then freezing the active-layer morphology.

The PCE of OSCs has increased enormously in the past fifteen years, thanks to the introduction of NFAs.[115] Unlike fullerene acceptors, this family of acceptors absorbs light in the VIS-NIR region of the solar spectrum, increasing the solar harvest of NFA-based devices and producing high PCE exceeding 19%.[18,101,102] These acceptors can more easily be chemically modified than fullerene acceptors because of their anisotropic structure, which has improved both their PCE and stability.[18,103–105,116–118] Refs. [119, 120] detail the synthesis principles of numerous NFAs used in OSCs, while ref. [121] focuses specifically on fused-ring electron acceptors, highlighting their structural variability. Among NFA, a vast number of molecular modifications on ITIC derivatives have been devoted to

© 2024 The Author(s). Advanced Optical Materials published by Wiley-VCH GmbH

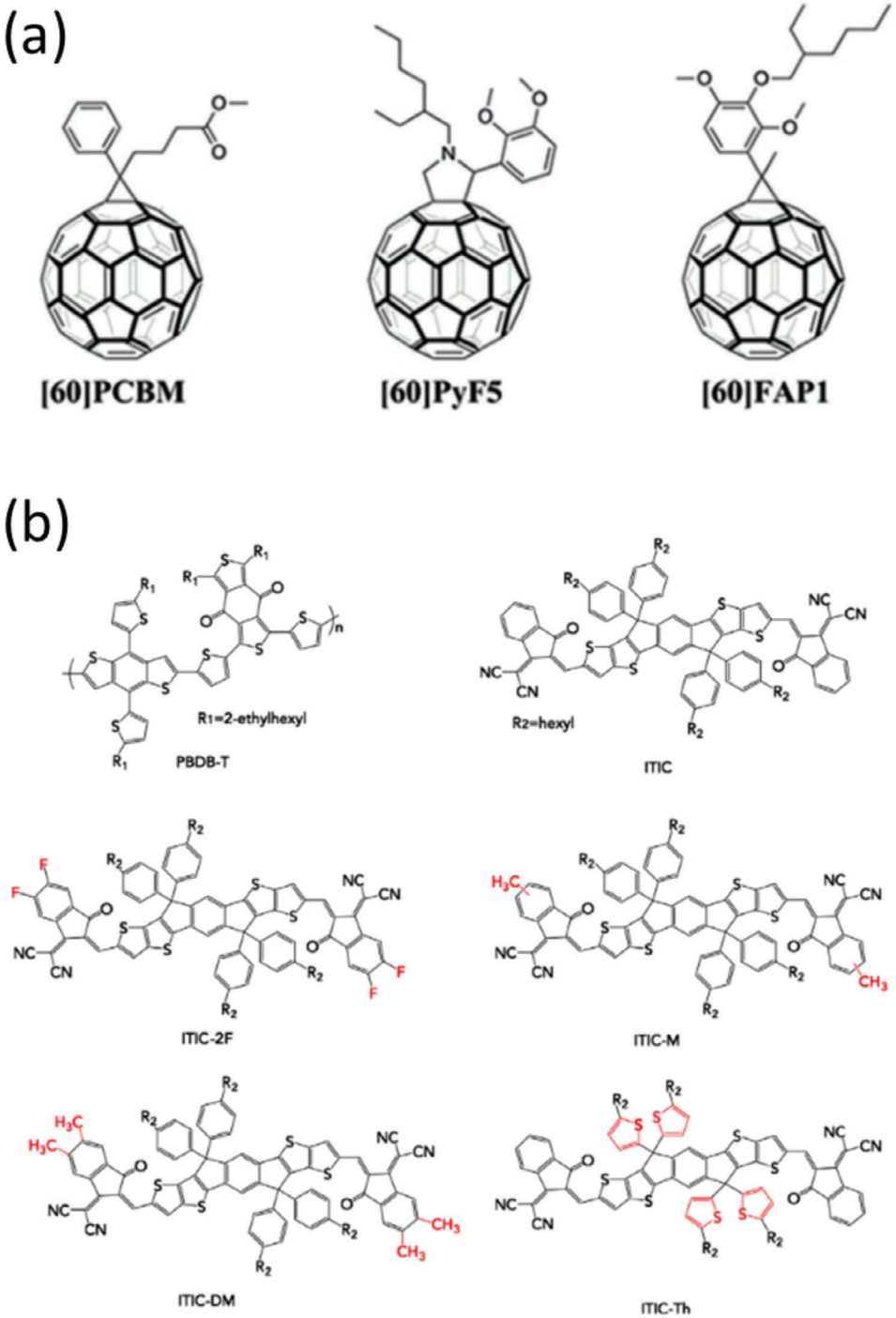

Figure 5. Chemical structures of a) novel fullerene acceptors[108] and b) molecular modifications on ITIC derivatives[18] for improved PCE and stability in OSCs. Reproduced with permission.[18,108] Copyright 2017, Wiley-VCH and 2019 Elsevier.

improving both the PCE and stability of NFA-based OSCs.[69,122] Du et al. reported a potential lifetime approaching 10 years with ITIC-family-based OSCs.[18] As shown in Figure 5b, a subtle molecular structure modification of ITIC on its side chain or end-groups resulted in a different photostability; for example, fluorination and methylation of the end groups were respectively found to stabilize and destabilize the molecules from light soaking.[18] The authors also discovered fluorination of both the donor and acceptor units as a route for stable OSCs. Crystallization of ITIC in a D/A BHJ blend is one of the factors that has hampered the stability of NFA-based OSCs due to phase separation, which significantly reduces photogeneration in the

© 2024 The Author(s). Advanced Optical Materials published by Wiley-VCH GmbH

device. Xin et al. found that the crystallinity of ITIC can be modified by fluorinating the acceptor at the ortho- and meta-alkyl positions of the phenyl side chains, giving rise to oF-ITIC and mF-ITIC, respectively.[104] After 96 h of annealing at 150 °C, the PCE of OSCs with PBTIDBTT:ITIC, PBDTIDBTT:oF-ITIC, and PBDTIDBTT:mF-ITIC dropped by 18, 33, and 8%, respectively, due to the high crystallinity of oF-ITIC and ITIC, which favored aggregate formation due to thermal stress.[104] Furthermore, a comprehensive stability-structure relationship of families of ITIC-based acceptors with fused, semi-fused, and non-fused molecular structures indicated that a thick brick-like structure could be created in a non-fused NFA, PTIC.[103] This dense structure inhibits photoisomerization, which occurs when the C═C and C—C bonds rotate concurrently, making the C═C bond more reactive to photodegradation, allowing ITIC-based polymers to retain 72% of their initial PCE while fused and semi-fused polymers could retain only 20–30% after 500 h of irradiation due to significantly reduced trap-assisted recombination in the non-fused NFA-based device. Similarly, the molecular packing of ITIC was successfully tuned by replacing two of the sulphur atoms in its core unit with selenium, increasing its intermolecular interaction and significantly increasing the lifetime of the NFA-based device to 5600 h compared to 400 h for ITIC.[123]

Apart from ITIC, the most widely used NFA, alternative small molecule and polymer NFAs that succeeded in delivering stable devices include NOE10 (a linear oligoethylene oxide side-chain modified naphthalene diimide-based polymer), TBD-PDI-Se, N2200, Y6, and IDTBR (a rhodanine-terminated small molecule acceptor).[105,124–127] The work of Clarke et al. revealed that the photostability of O-IDTBR, EH-IDTBR was superior compared to ITIC, and ITIC-M as the latter suffers from significant degradation due to the twisting and breakage of chemical bonds that result in undesirable conformations for charge generation and transport.[125] Chlorination was able to prevent NFA, like Y6, from self-assembling. This enhanced the thermal stability of the PM6:Y6-based device since the chlorinated acceptor's backbone conformation remained unchanged over an extended 100-h annealing period at 100 °C.[105]

Another major improvement is the use of two acceptors in a ternary blend to effectively combine the benefits of the two acceptors, such as a larger absorption cross-section of the NFA and excellent electron mobility of fullerene-based acceptors. Such ternary blends have the additional benefit of improving the stability of OSCs.[110,128–133] The evolution of trap-assisted recombination in IEICO-4F-based fullerene-free solar cells due to photodegradation could be retarded by adding 10% $PC_{71}BM$ to the active layer of PTB7-Th:IECO-4F, which resulted in a ternary blend with a remaining PCE that increased from 50% to 80% after 500 h of irradiation.[130] Interestingly, this finding revealed that the improvement was due to the synergistic interaction between the components rather than the stability of the single components. In another work, the addition of PCBM to an all-polymer solar cell based on PBDTTTPD: P(NDI2HD-T) revealed that the stability of the ternary blend devices deteriorated with increasing PCBM concentration.[110] A small percentage (30%) was found to be an optimum concentration of the fullerene to improve the performance of the ternary device while maintaining comparable stability with the binary all-polymer solar cells. However, upon increasing the concentration of PCBM, it was found that a small portion of PCBM nucleated to form large aggregates that impede charge percolation, resulting in a high loss of PCE with thermal stress. Similarly, the addition of crystalline acceptors such as PZ1 and O-IDTBR was found to inhibit the aggregation of non-fullerene acceptors and reduce trap-assisted recombination, thus maintaining the PCE of the devices over a longer period,[129,132] indicating that the incorporation of a third component in binary devices may serve as an important strategy in enhancing the stability of OCSs. Another all-polymer ternary blend comprising two donors and a single acceptor unit, PBDT-TAZ:PTB7-Th:NOE10, revealed burn-in-free thermal stability and retained 98% of its initial PCE after 300 h of heating at 65 °C.[124] This excellent stability was mainly attributed to NEO10, which has a stable morphology.

An important challenge with NFAs is the photocatalytic reactivity of ZnO, a common ETL material in inverted device structures (see Section 2.2). Charge carriers generated in ZnO upon UV photon absorption can reduce or oxidize adjacent molecules directly or via the formation of ROS. The T_{80} lifetime due to this rapid degradation could be increased five-fold by using ICBA as a fullerene additive in a binary blend of PBDB-TF:IT-4F OSCs.[133]

Tailoring the structure of acceptors to tune their LUMO level is another strategy to stabilize OSCs. The LUMO level of acceptors controls triplet-mediated singlet oxygen generation in OSCs. Distler et al. reported that a fullerene with a LUMO energy of −3.75 eV presented P3HT:fullerene-based OSCs with optimal stability.[134] A comprehensive work of Speller et al. highlights the importance of the LUMO of the acceptors in suppressing triplet-mediated singlet oxygen generation in BHJ OSCs where a deep-lying LUMO level was found to favorably inhibit such degradation, as shown in **Figure 6**b.[135] Two additional functions of fullerene that further enhance the stability of OSCs are its radical scavenging function, which similarly depends on its LUMO level, and its UV-light-screening function, which inhibits photoinduced chain breaking in the polymers.

4.1.2. Donor Materials

In both fullerene- and NFA-based OSCs, the contribution of the conjugated polymer or small molecule donor to both stability and performance is significant. Hence, considerable effort has been invested in introducing new polymer structures to improve OSC devices in terms of both PCE and stability. The donor:acceptor BHJ active layer can be stable if both the donor and the acceptor are stable while maintaining an interpenetrating-network morphology.

The stability of donor polymers can be improved by engineering the side chains, albeit to a limited extent. The solubility of polymers is strongly dependent on the side chains with varying lengths, locations, bulkiness, and kinds, which will ultimately affect both PCE and OSC stability. However, side-chain breakage caused by deterioration is a common scenario and can result in the creation of charge traps that can lead to further degradation. A UV-light degradation study on four PBDTTT-based polymers, each of which comprises benzodithiophene-co-thienothiophene (BDT-TT) as the backbone and a different type of side chain (structures shown in Figure 5), found that OSCs containing alkoxy side-chain substituted polymers are more

© 2024 The Author(s). Advanced Optical Materials published by Wiley-VCH GmbH

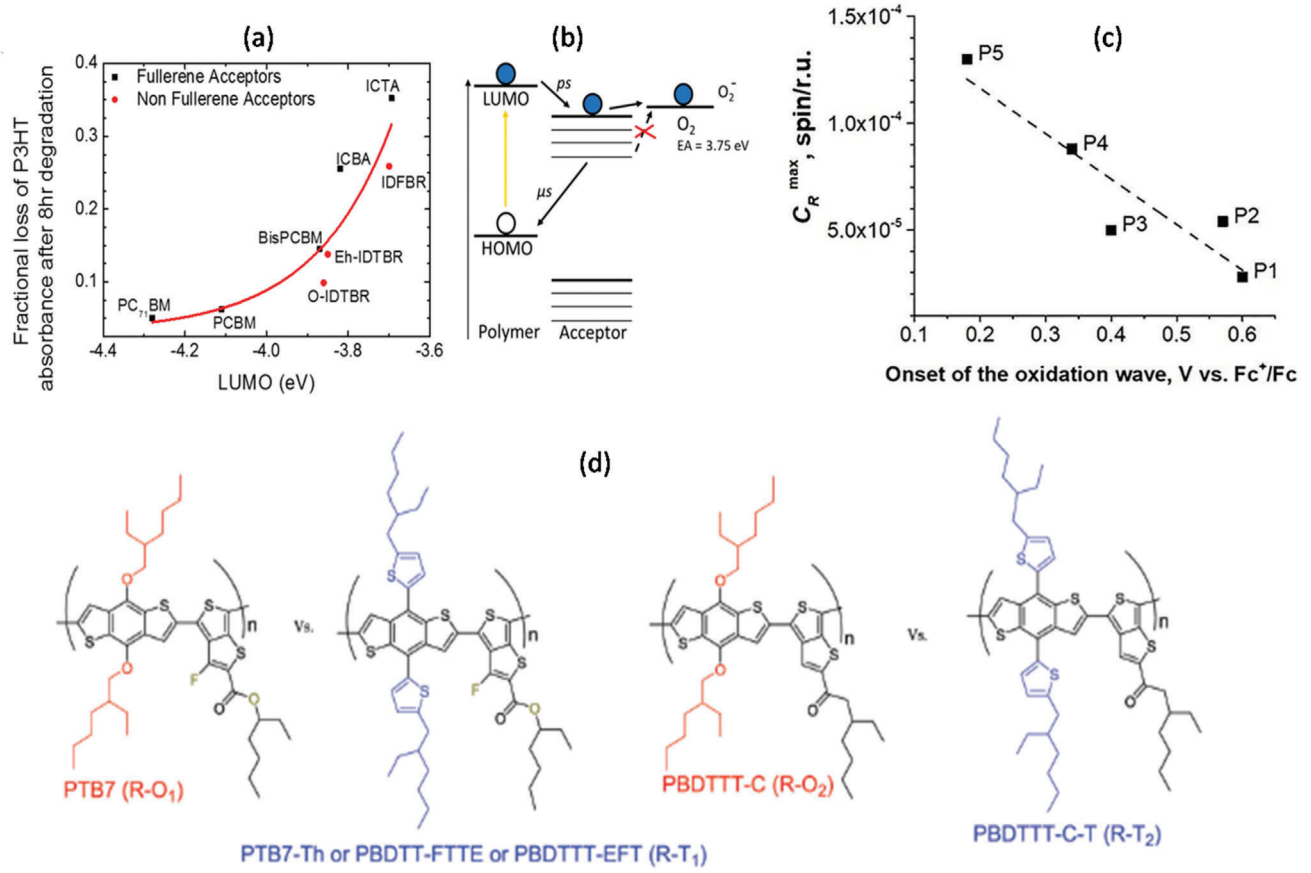

Figure 6. a) Fractional losses of P3HT absorbance peaks in blend films after 8 h of exposure under AM1.5G illumination in dry air (RH < 40%) as a function of the measured LUMO level of the acceptors, fitted with an exponential growth function $y = y_0 + Ae^{(x-x_0)/t}$ (red line) and b) proposed degradation mechanism, namely, the photodegradation of P3HT caused by the formation of superoxide (O_2^-) via electron transfer from the LUMO levels of the acceptors to molecular oxygen (O_2), which has an electron affinity of 3.75 eV. Reproduced with permission.[135] Copyright 2019, American Chemical Society. c) Donor HOMO and photooxidation: maximum radical species concentration per repeating unit (as a measure of oxidation) versus electrochemical oxidation potential (related to the HOMO energy). Reproduced with permission.[136] Copyright 2021, European Chemical Societies. d) Schematic illustration of morphological evolution with thermal stress. Reproduced with permission.[137] Copyright 2017, Royal Society of Chemistry.

stable than those having alkylthienyl-substituted polymers, possibly due to a photochemical reaction induced by the UV light.[137] The authors determined that the photochemical reaction of the alkylthienyl side chains could result in polymer disintegration, thus impeding charge transport and consequently the stability of the devices. This effect was, however, less significant with the alkoxy-substituted polymers. A follow-up study reported that the generation of free radicals and deep traps may explain the faster degradation of the PBDTTT polymers with alkylthienyl side chains.[138] Desalegn et al. demonstrated the importance of optimizing the alkyl side-chain length to control the stability of thiophene-bridged thieno-thiophene polymers against thermal stress.[139] Oxidation of the backbone structure of a donor polymer could be inhibited by using antioxidant side chains such as butylated-hydroxytoluene units.[140] Saito and Osaka reported the effect of regularity in the placement of side chains. By demonstrating the difference in their work, they found that less regular side chain placement maintains the structural ordering of the active layer during thermal degradation, successfully lowering the degradation of the device compared to the device based on a polymer with regularly placed side chains.[76] In addition to the side chains, the atom that the side chain is attached to on the main backbone was found to influence the stability of the OSCs.[141]. Apart from common side chains like alkyl or alkoxy groups, fluorination, sulfonylation, and chlorination[142] are often employed to improve the performance of OSCs mainly by improving the V_{OC}. However, these substitutions might worsen the UV-stability of the device.[143]

Rigidifying the active-layer morphology using chemical crosslinkers has been identified as another viable route to enhance the stability of OSCs. Bromide, vinyl, acrylate, azide, and oxetane are popular crosslinking units.[144] Yang et al. recently reported that crosslinking of PTPDBDT-based OSCs led to a considerable enhancement in both the PCE (from 7.56% to 12.18%) and the stability.[145] Another study showed that OSCs containing a vinyl-functionalized PBDTTPD polymer with a 2.5% vinyl content retained 91% of their initial PCE after thermal treatment at 150 °C for 40 h, which was markedly better than devices containing non-crosslinked polymers.[106] Similarly, vinyl-functionalization of a D:A polymer blend consisting of benzodithiophene-thienopyrroledione (BDT-TPD) and naphthalenediimide (NDI) units, respectively, substantially slowed

© 2024 The Author(s). Advanced Optical Materials published by Wiley-VCH GmbH

down the long-term thermal stress-induced degradation due to the stabilization of the morphology.[146]

The crystallinity of polymers can be one of the factors driving optimal phase segregation in donor-/acceptor-based OSCs, which is a determining factor for the final PCE of the device. This was demonstrated using two photostable donors with different polymer crystallinities: the more crystalline polymer was found to be more photostable due to its better electron and hole mobility resulting from fewer charge traps.[147] However, only a limited amount of crystallization favors stability because excessive aggregation of one of the domains in the active layer hampers exciton dissociation and charge transport.[148]

The electrochemical oxidation potential of polymers plays a crucial role in the photooxidation of the material. An electron spin resonance (ESR) study on 16 polymers, each with a different HOMO energy level, revealed a linear anticorrelation between the onset of oxidation of the conjugated polymers and their photooxidation tendency (Figure 6c), suggesting polymers with deeplying HOMO energy levels are less susceptible to photooxidation and may considerably enhance the photostability of devices.[136] A number of strategies including coupling weak donor units[149] and introduction of strong electronegative atoms such as fluorine and chlorine can effectively increase the delocalized electrons in the backbone resulting in a deeper HOMO level,[150–152] which consequently may reduce photooxidation of the polymers.[153]

4.1.3. Active-Layer Morphology

The chemical breakdown of the donor and acceptor and the evolution of the morphology, which does not favor both charge generation and transport, are the two main degrading processes in the active layer. An exciton generated must reach a D/A interface within its diffusion length to dissociate into free charge carriers. These charge carriers will be able to reach the electrode if there is an uninterrupted percolation path toward the respective electrode. However, the morphology of the active layer is generally a metastable state that readily evolves to a thermodynamically stable state even at room temperature.[154,155]

The main approaches used in limiting the evolution of the active-layer morphology include molecular structure engineering of both donor and acceptor units, reduction of their crystallinity, crosslinking of the active-layer materials, and interface engineering.[106,146,156,157] For example, the mobility of polymers above the glass transition temperature (T_g) and subsequent thermal degradation can be restricted by creating a polymer network that stabilizes the active layer's morphology due to an increased T_g. Hydrogen bonding within the polymer networks has been identified as an effective mechanism for producing rigid polymer fibers with high T_g, which enhances thermal stability.[158] Additionally, this process can initiate a molecular lock that promotes polymer aggregation, effectively "freezing" the active layer's morphology.[159]

Various studies have shown that the addition of a third component to form a ternary blend stabilizes the morphology of the active layer by inhibiting aggregation[129] and enhancing the crystallinity,[128,132] while at the same time providing an optimized charge thermodynamic process with delayed fluorescence.[160] However, an opposite trend was observed when adding a high concentration of PCBM as a third component in a binary all-polymer OSC, where the formation of PCBM crystallites drastically reduced the D/A interface and led to a significant drop in PCE.[110]. The schematics of the evolution of such morphology are shown in **Figure 7a**. This change in the phase separation in OSCs with PCBM is mainly attributed to the high diffusion coefficient of the isotropic fullerene acceptors.[117]

In NFAs, de-mixing from the intermixed region of the active layer due to degradation is not visible due to their much smaller diffusion coefficient.[117] As aggregation and/or crystallization in these devices only cause local crystallization of the NFA on a small scale, which is not easily identifiable using common techniques, morphological evolution in these situations is not evident. However, these small aggregates have a considerable impact on the device's electron mobility, leading to an electron trap that lowers the FF. Du et al.'s schematic clearly shows the local aggregation of NFA in contrast to the FA, which forms large phase-separated aggregates that reduce the D/A interfaces, as depicted in Figure 7b.[117]

In contrast to the typically utilized D/A-based devices, a frozen morphology could be achieved through the one-pot synthesis of a multicomponent polymer photoactive layer for OSCs, which is both highly efficient and stable with a T_{80} lifetime of more than 1000 h.[161] In these single-component OSCs, aggregation of each component is highly reduced, promoting entanglement of each chain and endowing the three-in-one polymer (e.g., PM6-D18-b-PYIT-based device) with superior efficiency and stability than the corresponding binary- and ternary-component-based devices.[162]

4.2. Electron- and Hole-Transport Layers

In an OSC, the active layer sandwiched between two symmetric electrodes forms a Schottky barrier due to the difference in work functions, which often results in a significant loss in V_{OC}.[163,164] To alleviate this issue, electron- and hole-transport layers (E/HTLs) are commonly inserted at the interface between the active layer and the electrodes. These layers have several advantages, including their ability to modify the work function of the metal electrodes, effectively increasing the V_{OC} of the device while enhancing charge extraction.[165] Additionally, they help prevent extrinsic degradation of the active materials.[166] Transport layers can consist of materials such as inorganic, organic intralayers, and organic-inorganic hybrids.[167–169]

4.2.1. Electron-Transport Layers (ETLs)

The morphology of the active layer of an OSC is influenced by the interface between the active layer and the E/HTLs. In contrast to the traditional geometry, an inverted structure has better stability, which is usually unrelated to the chemical degradation of the active-layer materials. The use of stable oxides as ETL, such as ZnO, is one of several factors that contribute to the stability of inverted devices. A study on DBP/C_{70}-based OSCs fabricated both in conventional and inverted geometries using MoO_3 as ETL and BCP as ETL, demonstrated that comparable stability could be achieved when a BCP-Ag complex was used as ETL in the conventional device.[170]

© 2024 The Author(s). Advanced Optical Materials published by Wiley-VCH GmbH

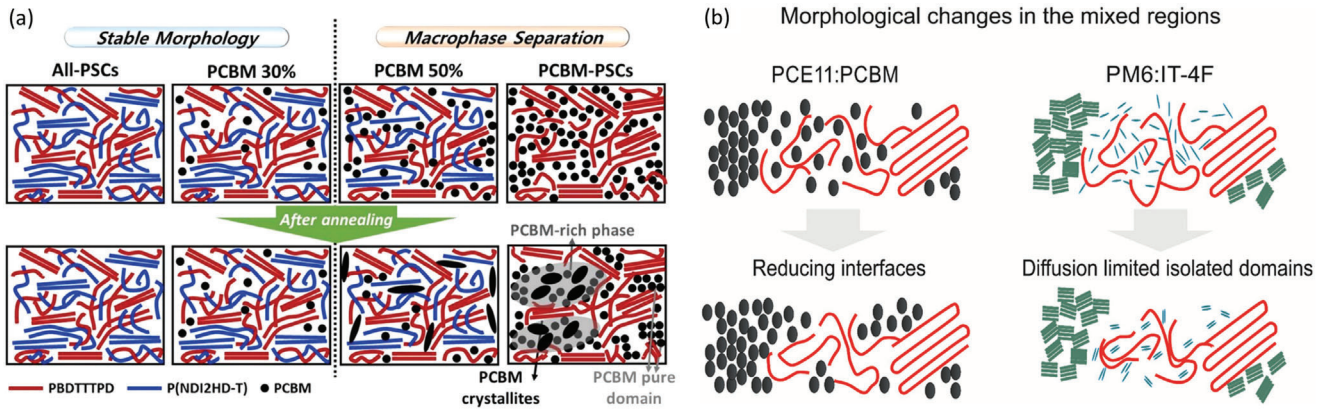

Figure 7. Schematic illustration of morphological evolution with thermal stress: a) Blend films of all-PSC, ternary-PSC, and PCBM-PSC before and after thermal annealing. Reproduced with permission.[110] Copyright 2017, American Chemical Society. b) Local aggregation of a non-fullerene acceptor in contrast to a fullerene acceptor. Reproduced with permission.[117] Copyright 2020, Wiley-VCH.

ZnO is a commonly used ETL in inverted OSCs owing to its excellent transmittance, matching energy levels with common acceptors for electron transfer, and high conductivity. However, this ETL is filled with defects that lower the performance of the devices and eventually cause degradation in the device.[171] Surface defects in ZnO, such as oxygen vacancies and Zn^{2+} interstitials, can serve as recombination sites for charge carriers. Furthermore, surface defects can be sites for oxygen and water adsorption,[172] resulting in the generation of ROS upon electron transfer from the photo-excited active-layer material to the molecular oxygen adsorbed, which would eventually destroy the active-layer material. Modification of the ZnO layer to reduce the Zn interstitial can be a viable route to reducing the chemisorption of oxygen on the surface. A composite ZnO:$ZnWO_4$ ETL was found to reduce the Zn-interstitial defect density, resulting in a much better stability.[173] Yan et al. reported an improved UV exposure and environmental stability after coating ZnO with carbon nanomaterials, which was found to increase the hydrophobic nature of the ETL, effectively suppressing adsorption of oxygen.[174] Doping of the ZnO with metals such as Li, In, and Al was also found to reduce trap states[175–177] leading to enhanced stability and improved PCE. The roughness of the ZnO layer has also been found to play an important role in the stability of OSC devices,[178] thus making it one of the most commonly used ETLs.

Another issue that needs considerable attention is the UV-activated photocatalytic property of ZnO against NFAs, necessitating the use of passivation layers to suppress the photocatalytic degradation of NFAs in inverted OSCs. Another strategy exploits the radical-scavenging property of fullerenes: the device stability was shown to improve remarkably by adding fullerene derivatives to an NFA-based OSC as a third component, with ICMA giving the best result.[179] Alternatively, self-assembling monolayers can be used as interface modifiers of ZnO to reduce the photocatalytic properties of the ETL, thus simultaneously increasing the PCE, thermal, and photostability of OSCs.[157,180,181] Degradation of the ZnO layer also changes its work function, making extraction of electrons difficult. Polyethylenimine (PEI) mixed with ZnO was, however, found to effectively suppress these changes, with only minor changes observed in the electrical properties of ZnO:PEI compared to a ZnO ETL, resulting in an improved stability of P3HT:PCBM-based inverted OSCs.[182–184]

Other ETLs such as SnO_2 and TiO_2 are also used in OSCs. SnO_2 has superior charge conductivity and transparency compared to ZnO in addition to its excellent chemical stability against UV, making it more appropriate for NFA-based OSCs.[185,186] On the other hand, recent reports on OSC performance and stability using TiO_2[187,188] are partly attributed to its porous surface, which makes it difficult to get a good thin ETL, multiple-phase formation that readily changes by coating conditions, in addition to low-electron mobility.[189,190] Furthermore, TiO_2 degrades more rapidly under UV illumination, which causes photodoping by the chemisorbed oxygen, leading to unfavorable band bending for charge extraction. In addition, its photocatalytic property is the main cause of degradation when used in non-fullerene-based OSCs. Park et al. reported a UV-A insensitive TiO_2 ETL that was able to effectively suppress its photocatalytic effect on a non-fullerene-based OSC.[191] Small molecules such as PFN-Br, PFN-OX, PDINO, and PDINN are among the recently employed ETLs in OSCs.[192,193] Comparative work on the stability of aluminium-doped ZnO (AZO), PFN-Br, and PDINN ETLs coated as cathode (Al) buffer layers in a conventional geometry revealed that the device with AZO ETL had the longest shelf life of $T_{80} > 1200$ h and thermal stability of $T_{60} > 300$ h due to the morphological and thermal stability of the inorganic AZO materials over the organic PFN-BR and PDINN ETLs.[192] In their work, the authors stressed the relevance of cathode interlayer material selection as a novel route for quick scans for stability. The XPS results of Al- or Ag-coated glass soaked in AZO, PFN-Br, and PDINN in **Figure 8** demonstrate that the binding energy of electrodes soaked in the organic ETL has increased due to strong electrochemical reactions between them. In contrast, such an energy shift is not observed in AZO-soaked electrodes, indicating that no chemical reactions occurred, giving a more stable device. The perylenediimide (PDI)-based small-molecule acceptor PDINO has a π-delocalized planar structure, giving rise to a high electron affinity and a PCE of 17% when used as an ETL.[194] However, the morphology of the blend films coated over PDINO was found to be filled with spikes and streaks after being aged for 60 days, while the device without PDINO exhibited a smooth and

© 2024 The Author(s). Advanced Optical Materials published by Wiley-VCH GmbH

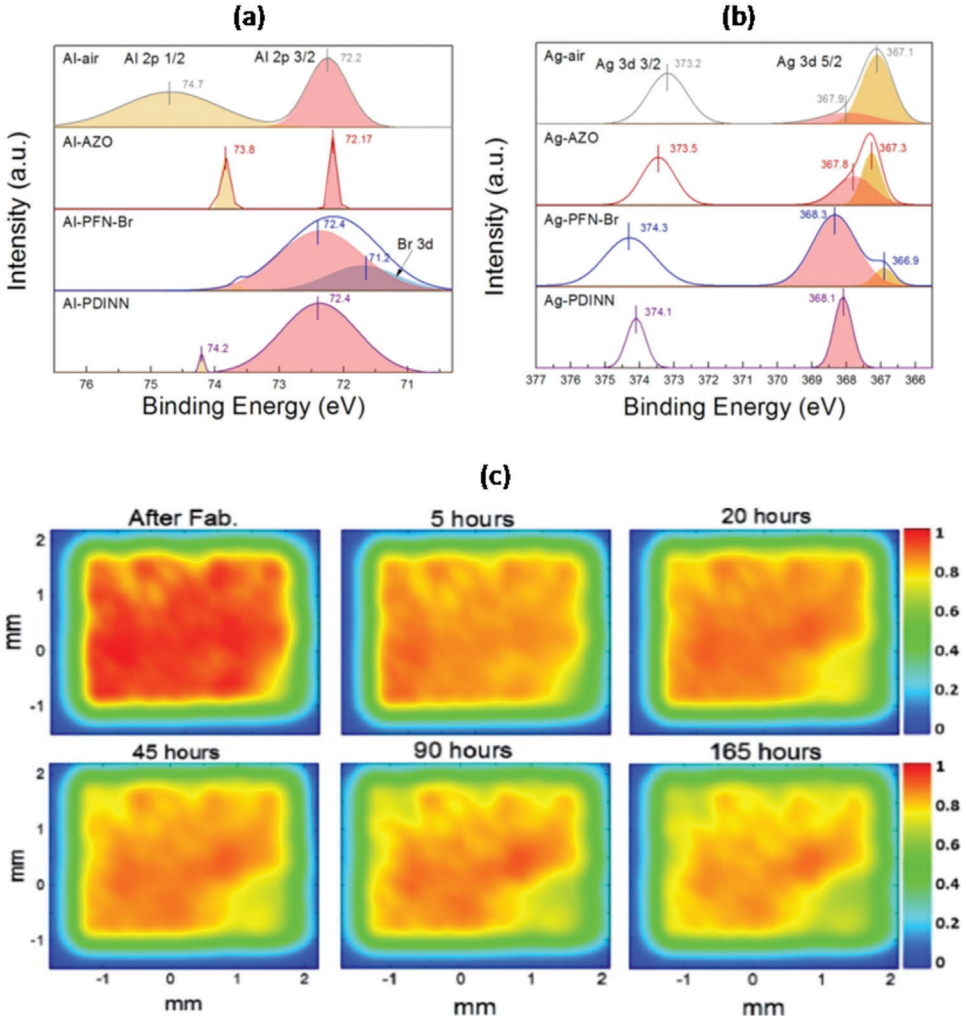

Figure 8. X-ray photoelectron spectra of a) Al and b) Ag cathodes coated with AZO, PFN-Br, and PDINN and compared to the control film Al-air (top). Reproduced with permission.[192] Copyright 2021, Elsevier. c) Photocurrent mapping of inverted P3HT:PCBM-based devices using MoO_3 as the HTL at different stages of thermal degradation. Reproduced with permission.[196] Copyright 2017, American Chemical Society.

uniform morphology. Consequently, the device with PDINO was found to lose 77% of its initial PCE after 140 days, while the device without it could maintain over 94%.[195]

4.2.2. Hole-Transport Layers (HTLs)

The most commonly used HTL, PEDOT:PSS, has many benefits, such as good hole-transporting ability, high transparency, and energy levels matching those of the HOMO of many donor polymers. However, this HTL is highly hygroscopic and acidic due to the insulator PSS chain. As a result, water ingress can easily modify its work function, resulting in a loss in PCE of the device. The commonly used transparent conducting electrode, ITO, can be corroded by the acidic nature of PEDOT:PSS. However, when MoO_3 was inserted between ITO and PEDOT:PSS, it was found to prevent moisture and oxygen ingression and etching of ITO, resulting in improved stability.[197] Additionally, barrier layers between ITO and PEDOT:PSS such as pH-neutral PEDO:PSS[198] and self-assembled monolayers can be employed to reduce the acidic attack on ITO.[34,199] Shen et al. neutralized the acidity of PEDOT:PSS by doping it with an organic base material, imidazole, to effectively improve the stability of PTB7-Th:PC_{71}BM-based devices.[200] Modifying the conformation of PEDOT:PSS was also found to contribute to the phase separation between PEDOT and PSS resulting in a better lifetime of the devices.[201] The stability of PEDOT:PSS-based OSCs can be further improved by incorporating chemically non-reactive carbon nanostructures,[202,203] V_2O_5 nanoparticles,[204] or the multifunctional additive 2,3-dihydroxypyridine (DOH).[201]

Many metal oxides such as MoO_3, V_2O_5 NiO_2, and WO_3 have been introduced as stable and efficient HTLs for OSC applications.[197,205,206] The stability enhancement of devices prepared using metal oxides as HTLs can be attributed to the reduction of anode/active-layer interface degradation,[207,208] stable active-layer morphology, stable electrodes to ensure good charge collection, and a stable HTL/electrode interface.[209] UV annealing was also shown to enhance the device stability

© 2024 The Author(s). Advanced Optical Materials published by Wiley-VCH GmbH

for solution-processed MoO_3 as the HTL as opposed to PEDOT:PSS.[205]

The stability of inverted devices, i.e., when metal oxides are used as the top electrode interlayer, is influenced by the contact between the active layer and the HTL. For instance, Hermerschmidt et al. reported significantly faster degradation when a P3HT:PCBM-based device was prepared using PEDOT:PSS/Ag as the top HTL/electrode as opposed to MoO_3/Ag.[196] The authors could improve the stability of the device fabricated with MoO_3/Ag by using PEDOT:PSS as an interlayer. A photocurrent mapping of the inverted device with MoO_3/Ag shown in Figure 8 revealed a fast photocurrent loss in the device after heating at 65 °C for 5 h. This loss could be suppressed by putting PEDOT:PSS as an interlayer between the active layer and MoO_3/Ag, confirming the direct contact of MoO_3 with the active layer as the cause of degradation.

In another report, the interface between MoO_x/Ag and the active layer could be improved by post-annealing of the device at 150 °C, yielding an environmental T_{80} lifetime of 20 750 h.[210] The authors attributed this long lifetime to the doping of S in the active-layer materials with Mo in the HTL, which led to a stable interface. It is worth mentioning that the control sample with no post-annealing lost 31.1% PCE in only 169 h, similar to the findings of Hermershmidt et al.[196]

4.3. Electrodes

The effective extraction of electrons and holes is one of the possible routes to achieve high efficiency in OSCs. The degradation of electrodes may shift their electrochemical potential compared to that of the active layer, increasing the probability of recombination of charge carriers. Unlike interlayers, suitable electrodes to substitute ITO, which is mechanically and chemically unstable, are still sought after. Many flexible substrates, including ultrathin glasses[211] and polymers such as polyethylene naphthalate (PEN)[212] and polyimide (PI),[213] have been among the few used to substitute the rigid ITO to improve the mechanical stability of OSCs.

The primary motivation for introducing flexible electrodes is to increase their mechanical durability. For instance, PI was incorporated into a graphene structure to produce a mechanically stable and flexible OSC with just 8% PCE loss after 10 000 cycles of bending.[213] This is mostly because the incorporation of PI assisted in preventing the graphene from delaminating under mechanical stress. Graphene electrodes can also be coated with an HTL such as PEDOT:PSS to improve charge extraction. However, the acidic nature of PEDOT:PSS is well recognized to damage the active layer, resulting in poor stability. Better HTLs, such as MoS_2, were used as a good substitute for coating on graphene to enhance both the efficiency and stability of flexible devices due to the lower resistance between the HTL and the active layer.[214] Furthermore, graphene and Ag nanowire composites can be used as transparent conductive electrodes due to their high conductivity and optical features. A graphene-Ag nanowire-/PEDOT:PSS electrode achieves a PCE of 13.44% in non-fullerene-based OSCs and has high mechanical stability, maintaining over 80% of its original PCE even after thousands of bends.[215]

Table 1. Overview ISOS protocols for dark and light-soaking conditions.

ISOS Protocol	Conditions	Temperature	Light Source	Relative Humidity
ISOS-D-1	Shelf storage	–	–	–
ISOS-D-2	Heat	65 °C/85 °C	–	Ambient (low)
ISOS-D-3	Damp and heat	65 °C/85 °C	–	85%
ISOS-L-1	Light	–	AM 1.5G	–
ISOS-L-2	Light and heat	65 °C/85 °C	AM 1.5G	–
ISOS-L-3	Light, heat, and damp	65 °C/85 °C	AM 1.5G	50%

The other commonly used flexible electrode is the highly conductive PEDOT:PSS, called PEDOT:PSS-PH1000, coated on PET substrates. PEDOT:PSS-PH1000 mixed with ethylene-glycol and treated with H_2SO_4 immersion can be used as a high work-function electrode in place of ITO to eliminate the acidic attack of PEDOT:PSS on ITO, resulting in a much higher photostability.[216] On the other hand, a higher wettability of digitally printed PEDOT:PSS on a PET substrate could be obtained when mixed with single-wall nanotubes doped with $HClO_4$, endowing it with better stability than ITO-based devices due to a stable charge injection.[217]

5. Testing Protocols for OSC Characterization

5.1. ISOS Protocols

Due to the importance of OSC stability and the need for commercialization, researchers worldwide are currently studying the stability of OSCs by measuring device performance under different conditions. This process involves scanning IV curves under solar simulators over some degradation period to extract PV parameters. However, comparing results from different labs is challenging due to various factors influencing device stability. To address this, standard protocols for different testing conditions were established at the 2010 International Summit on Organic Photovoltaic Stability (ISOS).[218] The consensus was based on an agreement among experts in the field of OPV on how to conduct and report degradation studies under controlled and repeatable conditions.[218] The ISOS protocols, designed primarily for laboratory-scale devices, aim to ensure the comparability of PV testing carried out at various laboratories, enable successful round-robin experiments, and improve the caliber and applicability of published data.[219–221] These protocols are divided into five groups: shelf-life or dark storage testing (ISOS-D), outdoor testing (ISOS-O), light-soaking testing (ISOS-L), thermal cycling testing (ISOS-T), and light-humidity-thermal cycling testing (ISOS-LT). The protocols can be used with both encapsulated and unencapsulated devices, as long as they are well-documented. Each area is further divided into three degrees of sophistication: basic, intermediate, and advanced, covering various levels of laboratory infrastructure.

For example, **Table 1** outlines the requirements for tests in the dark and under light-soaking conditions, with D referring to dark and L referring to light. There is an increase in the number of parameters to be regulated as the level of sophistication increases. The first test in dark conditions (ISOS-D-1) requires a sample to be placed on a shelf and evaluated regularly. ISOS-D-2 requires

© 2024 The Author(s). Advanced Optical Materials published by Wiley-VCH GmbH

the sample to be placed in an oven with temperature controlled at 65 °C or 85 °C. ISOS-D-3, the most sophisticated level, requires the sample to be placed in a special aging chamber with temperature control at 65 °C or 85 °C and relative humidity at 85%. For indoor laboratory light soaking, ISOS-L-2 or ISOS-L-3 require the device to be kept at 65 °C or 85 °C, while ISOS-L-3 additionally requires a relative humidity of 50%. Here, 1, 2, and 3 refer to the three different levels of sophistication, which evaluate different stress factors with respect to temperature and humidity. A complete elaboration of all the ISOS protocols is out of the scope of this review and interested readers are referred to ref. [218].

The ISOS-D dark storage tests examine solar cell resistance to oxygen, moisture, and atmospheric components, as well as severe temperatures. They are used to test thermal stability and accelerate deterioration induced by other factors.[222] The ISOS-D-2 test examines the effect of increased temperatures on device stability.[223–226] Monitoring ambient relative humidity is also critical, as dry and humid air represent different stress conditions for solar cells.[226,227] The ISOS-D-3 damp heat test therefore analyses the influence of humidity when devices are held at elevated temperatures.

It has been reported that the light-soaking experiments (ISOS-L) generate adverse changes in organic charge extraction layers, material intermixing, and ion exchange in solar cell layers.[228] The UV band of the solar spectrum is also of particular interest as it aids in OSC degradation and enhances the non-radiative recombination rate in OSCs based on mesoporous TiO_2.[228,229] The ISOS-L-1, ISOS-L-2, and ISOS-L-3 levels therefore assess these stress variables based on temperature and humidity.

The impact of natural solar illumination on device aging is investigated in outdoor stability studies (ISOS-O). These findings are critical for device operation and can provide accurate estimations of device longevity with respect to a given climate. ISOS-O-1 and ISOS-O-2 include frequent *I–V* curve measurements under illumination by a solar simulator and natural sunlight, respectively. ISOS-O-3 needs in situ maximum power point (MPP) tracking in natural sunshine as well as performance evaluations in a solar simulator. However, the results of *I–V* measurements and MPP tracking do not always coincide, even though they may show comparable tendencies.

Thermal cycling in the dark (ISOS-T) and light-humidity thermal cycling (ISOS-LT) evaluate degradation in PV devices induced by solar radiation, temperature, and humidity fluctuations. These tests apply to outdoor-dedicated PV technologies such as OSCs. The three levels of sophistication (ISOS-T-1, ISOS-T-2, and ISOS-T-3) simulate real-world conditions and drive failure processes related to layer or contact degradation. Depending on the available equipment, temperature cycling can range from basic hotplate activation in the ambient atmosphere to complicated temperature and humidity cycles in an environmental chamber.

5.2. Recent Progress In the Lifetime of OSCs

PCE is the most used parameter when comparing the performance of one solar cell to another. It can be defined as the ratio of energy production to incoming energy from the sun. Degradation in OSCs is evident as a drop in PCE over time, which may result from a variety of aging events, often driven by several factors including oxygen or moisture ingress, excessive heating, or solar radiation, the latter mostly owing to UV light.[230–232] Developments in encapsulating technologies have enabled efficient management of ambient-induced deterioration. As a result, solar irradiation-induced deterioration (i.e., photodegradation—see Section 3.1.2) remains one of the main obstacles to OSC commercialization.

Since PCE depends on the spectrum and intensity of incident sunlight as well as the temperature of the solar cell and the ambient humidity, a performance comparison of devices requires careful regulation of these parameters using the ISOS protocols elaborated in Section 5.1. However, the lifetimes reported in the literature are often recorded under different conditions and are therefore difficult to compare. This is illustrated in **Table 2**, which shows examples of recent degradation studies (from the past ~5 years) that reported performance and PV parameters. A broad range of degradation conditions were used, most of which deviated from ISOS protocols, and most studies did not report the corresponding device lifetimes. Since the active-layer material plays a crucial role in the lifetime of OSCs, we are including blends of both fullerene- and non-fullerene-based active layers in the table for comparison. Additionally, we present stability studies of state-of-the-art polymers, specifically focusing on PM6 and D18, which have achieved PCEs exceeding 18%. Since both the efficiency and lifetime of OSC devices are influenced by the active-layer area,[233–235] the area of the devices is also given, along with the PV parameters J_{SC}, V_{OC}, FF, and the efficiency before (F) and after (D) degradation.

Some studies have reported very stable OSCs, such as an NFA-based OSC with a predicted lifespan of around ten years[236] and an extraordinarily stable class of thermally evaporated single-junction, PBDB-T:OY3 active layer-based OSCs with an estimated extrapolated outdoor lifetime of up to 27 000 years.[237] However, these high stabilities were obtained at the expense of a relatively low PCE (ca. 8% and 6.7%, respectively). The ISOS protocols were also not properly followed, making it difficult to compare these results. Specifically, the devices with an estimated lifetime of about 10 years were obtained under continuous 1 sun illumination in a dry nitrogen atmosphere with a controlled O_2 level below 0.5 ppm and cell temperature maintained under 40 °C, while the extremely stable OSCs (27,000 years) were obtained after drastically accelerating the aging process by exposing the packaged cells (in an inert atmosphere) to white-light illumination intensities of up to 37 suns.

While these reports show significant progress in realizing stable OSCs, it is important to note that such stability results are usually obtained under controlled or idealized conditions, which often do not represent real-world operational environments well, where factors such as light, temperature fluctuations, humidity, and oxygen exposure are major sources of degradation. Furthermore, variations in material design, device designs, and testing protocols can result in varying stability outcomes among researchers. This again highlights the importance of the ISOS protocols discussed in Section 5.1 as they aim to offer a comprehensive understanding of both the progress made and the challenges that still need to be addressed for achieving universally stable OSC devices. Achieving both high efficiency and high stability is essential for future advancements.

© 2024 The Author(s). Advanced Optical Materials published by Wiley-VCH GmbH

Table 2. Recent advances in OSC degradation. Parameters are shown for fresh (F) and degraded (D) devices. See text for details.

Type of OSC	Active layer	Area [mm^2]	V_{OC} [V] F/D	I_{SC} [mA cm^{-2}] F/D	FF [%] F/D	PCE [%] F/D	ISOS protocol	T_{50}/T_{80}	Degradation conditions	Refs.
Fullerene-Based OSCs										
	DPB:C_{70}	10	0.85/0.36	5.8/4.90	71.2/23.3	3.50/0.68	ISOS-D-3	–	Darkness, 80 °C, 85 % relative humidity (RH)	[238]
	DPB:C_{70}	10	0.85/0.87	5.8/5.67	71.2/59.3	3.5/2.94	ISOS-T-3	–	Darkness, −40 °C, ambient humidity	[238]
	PDPPPTD:$PC_{61}BM$	6	0.885/0.906	10.14/9.56	68.62/54.26	6.16/4.70	–	–/200 h	Ambient, AM 1.5G simulated solar light, thermal annealing at 120 °C, for 10 mins	[239]
	P3HT:PCBM	9	0.59/0.53	9.65/8.75	57.1/54.0	3.27/2.50	–	–	Encapsulated and heated at 150 °C for 30 mins in a glove box	[240]
	PTB7-Th:$PC_{71}BM$	4.5	0.819/0.775	15.26/13.08	62/52	7.74/5.28	–	–	Ambient, photodegradation at room temperature under one-sun test conditions for 5 h, AM 1.5G	[241]
	DH6T:PCBM	14	0.30/0.66	0.63/1.55	26.2/29.3	0.06/0.30	–	–	Addition of 29.8 wt% Gaq3 dopant and thermal annealing at 180 °C, for 20 min in ambient air	[242]
Non-Fullerene-Based OSCs										
	PBDTTT-OFT:IEICO-4F	4	0.698/0.691	25.5/26.6	73.4/70.8	13.0/13.0	ISOS-D-2	–/1050 h	Darkness, thermal annealing at 85 °C, 30 % relative humidity (RH), glass-encapsulated	[243]
	PTB7-Th:IEICO-4F	–	0.72/0.66	23.03/15.67	65/51	10.77/5.28	ISOS-D-3	–	Operation under 85 °C for 5 h in an inert atmosphere without air in a nitrogen-filled glove box	[244]
	PTB7-Th:IEICO-4F	–	0.72/0.66	23.03/10.21	65/42	10.77/2.84	ISOS-D-3	–	Operation under 85 °C for 5 h in ambient air	[244]
	PBTIBDTT:ITIC	–	0.96/0.97	14.39/13.65	64.39/66.30	8.74/7.17	–	–	Accelerated thermal annealing at 150 °C, for 96 h, ambient	[77]

(*Continued*)

© 2024 The Author(s). Advanced Optical Materials published by Wiley-VCH GmbH

Table 2. (Continued)

Type of OSC	Active layer	Area [mm^2]	V_{OC} [V] F/D	I_{SC} [mA cm^{-2}] F/D	FF [%] F/D	PCE [%] F/D	ISOS protocol	T_{50}/T_{80}	Degradation conditions	Refs.
	PBTIBDTT:oF-ITIC	–	0.94/0.94	13.49/13.48	71.03/70.21	8.87/5.94	–	–	Accelerated thermal annealing at 150 °C for 96 h, ambient	[77]
	PBTIBDTT:mF-ITIC	–	0.96/0.96	14.53/14.34	68.11/67.79	9.39/8.67	–	–	Accelerated thermal annealing at 150 °C for 96 h, ambient	[77]
	PCE10:ITIC	7	0.80/0.75	14.05/9.11	64.82/42.69	7.28/2.93	–	–/221 h	Glass-encapsulated, continuous photo-illumination for 500 h in an ambient environment, AM 1.5G.	[245]
	PCE10:IDIC	7	0.78/0.76	12.83/11.83	61.07/54.12	6.12/4.90	–	–/558 h	Encapsulated, ambient, AM 1.5G, photoaging after 500 h	[245]
	PCE10:EH-IDT	7	0.99/0.99	14.86/14.75	62.13/60.33	9.17/8.82	–	–/2132 h	Encapsulated, ambient, AM 1.5G, photoaging after 500 h	[245]
	PTB7-Th:COi8DFIC	4.5	0.701/0.606	22.32/16.99	60/41	9.39/4.24	–	–	Ambient, photodegradation at room temperature under one-sun test conditions for 5 h, AM 1.5G	[241]
	PTB7-Th:COi8DFIC:$PC_{71}BM$	4.5	0.711/0.686	25.13/21.51	68/52	12.06/7.73	–	–	Ambient, photodegradation at room temperature under one-sun test conditions for 5 h, AM 1.5G	[241]
	PM7:TB-4Cl	–	0.882/0.862	21.69/22.09	71.17/71.78	13.62/13.67	–	–	Thermal annealing at 100 °C for 110 h in nitrogen	[246]
State-of-the-art OSCs										
	PM6:Y6	–	0.87/0.80	25.12/26.34	70.57/71.68	15.44/15.17	–	–	Addition of 30 wt% PAEF and thermal annealing at 80 °C for 5 mins	[80]
	PM6:Y6	–	0.854/0.837	24.27/25.05	74.00/75.85	15.34/15.90	–	–	Thermal annealing at 100 °C for 110 h in nitrogen	[246]

(*Continued*)

© 2024 The Author(s). Advanced Optical Materials published by Wiley-VCH GmbH

Table 2. (Continued)

Type of OSC	Active layer	Area [mm^2]	V_{OC} [V] F/D	I_{SC} [mA cm^{-2}] F/D	FF [%] F/D	PCE [%] F/D	ISOS protocol	T_{50}/T_{80}	Degradation conditions	Refs.
	PM6:TB-4Cl	–	0.848/0.835	22.99/23.20	75.20/75.17	14.67/14.56	–	–	Thermal annealing at 100 °C for 110 h in nitrogen	[246]
	PM6:N3	4.5	0.825/0.770	26.33/20.74	64.9/44.7	14.10/7.14	ISOS-L-3	–	Operation under simulated one-sun light and 85 °C for 5 h in ambient air	[247]
	PBDB-T:OY3	–	0.839/0.777	23.76/23.88	74.58/68.82	14.87/12.76	–	–/25000 h	Thermal annealing at 150 °C for 180 mins	[248]
	PM6-A5:Y6	–	0.84/0.73	26.16/26.50	63.03/55.93	13.85/10.82	–	–	Thermal annealing at 150 °C for 49.5 h	[249]
	PM6:Y6	3.96	0.852/ 0.654	25.7/23.5	71.8/64.3	15.7/9.87	–	–	Photodegradation with AM 1.5G for 1 h	[250]
	D 18:N3	–	0.83/0.83	27.35/27.32	77.19/ 76.91	17.56/17.50	–	–/200 h	Thermal annealing at 100 °C for 10 mins	[251]
	D18:DP-BTP	–	0.96/0.96	22.73/22.48	69.10/ 69.08	15.08/14.93	–	–/4963 h	Thermal annealing at 100 °C for 10 mins	[251]
	D18:N3:DP-BTP	–	0.87/0.87	27.95/27.84	78.50/ 78.15	19.07/18.86	–	–/1568 h	Thermal annealing at 100 °C for 10 mins	[251]

6. Challenges and Future Outlook

As reported, significant progress has been made in the field of OSCs, with photovoltaic PCE increasing from 0.001% to about 20%.[252] However, efficiency alone is insufficient for the commercialization of OSCs. Some of the challenges to be addressed include the high cost of light-harvesting materials, which are complex and require multiple procedures to produce pure materials.[253] As a result, the most efficient materials are synthesized on a small scale, allowing for mostly laboratory testing. Commercialization, however, necessitates considerable upscaling for widespread deployment. Since the material cost increases roughly linearly with the number of synthesis steps,[254] low-cost OSC materials are of primary importance. Such materials include molecules with basic chemical structures and simple synthetic techniques, for example, non-fused materials that do not require expensive and complicated ring-closure procedures.[255] One such example is a two-step synthesis of three simple non-fused electron acceptors, which still gave competitive PCEs of 10.27% and 13.97% for single and tandem OSCs, respectively.[256] PTQ10 is another example of a simple structure synthesized through a two-step reaction, which has given rise to an excellent PCE of 16.53%.[257,258] Early-stage OSC molecules like P3HT, PPV, and PTV are also worth considering due to their low-cost synthesis. However, OSCs made from simple structural materials typically perform poorly compared to those made from complex fused structures. As a result, molecular structure optimization is critical for improving the performance of OSCs made from simple structural materials.

In addition to achieving high PCEs in small-area OSCs, device engineers should focus on exploring novel technologies for large-area fabrication. Large-area OSC processing procedures differ significantly from laboratory fabrication approaches in terms of the transition from solution to solid film. To obtain wide-area OSCs with high PCE, it is crucial to explore the mechanisms involved in the morphological evolution process.

Numerous factors contribute to the instability of OSCs, the most prominent of which are oxygen, water, irradiation, heating, metastable morphology, diffusion of electrode and buffer layer materials, and mechanical stress (see Section 3). Light-induced degradation can result in photochemical and photophysical changes,[259] while high working temperatures can induce nanomorphological evolution.[260–262] Air instability and burn-in degradation are other concerns, with the cause of burn-in degradation still unclear even though researchers have reported many possible reasons such as the dimerization of fullerene-based acceptors, trap-state-assisted charge recombination, the broad polydispersity of polymer donors, and impurities in materials.[263–265] However, some studies have demonstrated stable OSCs, such as NFA-based OSCs with a predicted lifetime of around ten years[236] and single-junction OSCs with an estimated outdoor lifetime of over 27 000 years.[237] Nonetheless, achieving long-term stability in real-world situations remains a substantial difficulty and requires more concerted, interdisciplinary cooperation to overcome it.

Improved stabilization of the active layer is the most critical need. The kinetically mixed donor and acceptor materials are usually thermodynamically unstable.[263,266] External stress, such as thermal stress or illumination, usually causes unfavorable

© 2024 The Author(s). Advanced Optical Materials published by Wiley-VCH GmbH

microstructure evolution, resulting in performance losses.[91,263,267] To overcome this instability, OSCs based on single-component materials (SCMs), which have a chemically bonded donor and acceptor moiety in a single molecule or polymer, are an elegant solution. This chemically-connected structure prevents donors and acceptors from separating on a broad scale, resulting in greater morphological stability. These SCMs can also ensure processes including exciton formation and dissociation as well as charge transport, unlike the traditional BHJ idea that requires two materials (an independent donor and acceptor).[268,269] OSCs based on SCMs eliminate the issue of limited exciton diffusion lengths by generating and dissociating excitons in the same polymer or molecule. Exciton dissociation efficiency is expected to be high due to the high possibility of encountering a D/A interface. SCMs therefore offer significant advantages over the BHJ concept, including simplified device fabrication and stabilization of the active-layer morphology by suppressing significant phase separation, which is desirable for large-scale applications.[270,271] Nonetheless, developing suitable SCMs is challenging due to their rather complex synthesis and the morphological adjustments required for efficient nanophase separation.

The commercialization of OSCs necessitates a substantial improvement in their morphological stability without sacrificing their PCE. Since photooxidation is a key photodegradation mechanism, methods such as proper encapsulation, the use of radical scavengers and singlet oxygen quenchers (i.e., antioxidants), and UV polymer stabilizers to delay their photooxidation are important strategies. It is of note that similar protection against the deleterious effects of molecular oxygen has been well-established in natural photosynthetic systems for as long as they have been populating the earth, and biomimicry of some of the natural mechanisms is a promising way to enhance the stability of OSC active layers. Other promising methods include freezing the morphology of the active layer, material modification, and stabilizing the electrodes.

Finally, there is an important place for biodegradable (organic) materials in our green economy. Even though their lifespan may not be as attractive as high-stability materials, they address the rapidly increasing environmental concern of solar panel waste—the accumulating waste of solar panels that have reached the end of their lifecycles. Although oxygen and water are among the main factors causing OSC degradation, they are important factors in the biodegradation of materials. Therefore, to ensure effective end-of-life degradation, it would be sufficient to only retard oxygen- and water-induced degradation of functional OSC materials instead of trying to prevent the degrading impact of oxygen and water altogether.

Acknowledgements

This work is based on the research supported in part by the National Research Foundation of South Africa Grants No. PMDS22063029254 (LTN) and 120387 and 137973 (TPJK), the African Laser Centre Project No. HLHA23X (LTN) and HLHA25X (NAT and TPJK), the German Academic Exchange Service (DAAD) Research Grants – Short-Term Grants, 2024 (91897176) (LTN), the Rental Pool Program of the Council for Scientific and Industrial Research's Photonics Centre, South Africa (LTN and TPJK), and the National Institute for Theoretical and Computational Sciences (NITheCS), South Africa (NAT and TPJK).

Conflict of Interest

The authors declare no conflicts of interest.

Keywords

degradation mechanisms, ISOS protocols, organic photovoltaics, organic polymer stability

Received: August 21, 2024
Revised: December 5, 2024
Published online: December 26, 2024

[1] B. Qu, S. R. Forrest, *Appl. Phys. Lett.* **2018**, *113*, 5.
[2] R. Abbel, Y. Galagan, P. Groen, *Adv. Energy Mater.* **2018**, *20*, 1.
[3] M. Riede, D. Spoltore, K. Leo, *Adv. Energy Mater.* **2021**, *11*, 1.
[4] J. Yuan, Y. Zhang, L. Zhou, G. Zhang, H.-L. Yip, T.-K. Lau, X. Lu, C. Zhu, H. Peng, P. A. Johnson, M. Leclerc, Y. Cao, J. Ulanski, Y. Li, Y. Zou, *Joule* **2019**, *3*, 1140.
[5] J. Yuan, T. Huang, P. Cheng, Y. Zou, H. Zhang, J. L. Yang, S.-Y. Chang, Z. Zhang, W. Huang, R. Wang, D. Meng, F. Gao, Y. Yang, *Nat. Commun.* **2019**, *10*, 570.
[6] Y. Lin, J. Wang, Z.-G. Zhang, H. Bai, Y. Li, D. Zhu, X. Zhan, *Adv. Mater.* **2015**, *27*, 1170.
[7] B. A. Abdulahi, X. Li, M. Mone, B. Kiros, Z. Genene, S. Qiao, R. Yang, E. Wang, W. Mammo, *J. Mater. Chem. A* **2019**, *7*, 19522.
[8] J. Fu, Q. Yang, P. Huang, S. Chung, K. Cho, Z. Kan, H. Liu, X. Lu, Y. Lang, H. Lai, F. He, P. W. K. Fong, S. Lu, Y. Yang, Z. Xiao, G. Li, *Nat. Commun.* **2024**, *15*, 1830.
[9] C. He, Y. Pan, Y. Ouyang, Q. Shen, Y. Gao, K. Yan, J. Fang, Y. Chen, C.-Q. Ma, J. Min, C. Zhang, L. Zuo, H. Chen, *Energy Environ. Sci.* **2022**, *15*, 2537.
[10] Y. Wei, Z. Chen, G. Lu, N. Yu, C. Li, J. Gao, X. Gu, X. Hao, G. Lu, Z. Tang, J. Zhang, Z. Wei, X. Zhang, H. Huang, *Adv. Mater.* **2022**, *34*, 2204718.
[11] D. Li, N. Deng, Y. Fu, C. Guo, B. Zhou, L. Wang, J. Zhou, D. Liu, W. Li, K. Wang, Y. Sun, T. Wang, *Adv. Mater.* **2023**, *35*, 2208211.
[12] S. Guan, Y. Li, C. Xu, N. Yin, C. Xu, C. Wang, M. Wang, Y. Xu, Q. Chen, D. Wang, L. Zuo, H. Chen, *Adv. Mater.* **2024**, 2400342.
[13] L. Zuo, S. B. Jo, Y. Li, Y. Meng, R. J. Stoddard, Y. Liu, F. Lin, X. Shi, F. Liu, H. W. Hillhouse, D. S. Ginger, H. Chen, A. K.-Y. Jen, *Nat. Nanotechnol.* **2022**, *17*, 53.
[14] Z. Zheng, J. Wang, P. Bi, J. Ren, Y. Wang, Y. Yang, X. Liu, S. Zhang, J. Hou, *Joule* **2022**, *6*, 171.
[15] A. Bosio, S. Pasini, N. Romeo, *Coatings* **2020**, *10*, 344.
[16] M. Powalla, S. Paetel, E. Ahlswede, R. Wuerz, C. D. Wessendorf, T. Magorian Friedlmeier, *Appl. Phys. Rev.* **2018**, *5*, 041602.
[17] L. Duan, A. Uddin, *Adv. Sci.* **2020**, *7*, 1903259.
[18] X. Du, T. Heumueller, W. Gruber, A. Classen, T. Unruh, N. Li, C. J. Brabec, *Joule* **2019**, *3*, 215.
[19] P. Jiang, L. Hu, L. Sun, Z. Li, H. Han, Y. Zhou, *Chem. Sci.* **2022**, *13*, 4714.
[20] A. A. Mohapatra, M. Pranav, S. Yadav, C. Gangadharappa, J. Wu, C. Labanti, J. Wolansky, J. Benduhn, J.-S. Kim, J. Durrant, S. Patil, *ACS Appl. Mater. Interfaces.* **2023**, *15*, 25224.
[21] L. Yu, D. Qian, S. Marina, F. A. A. Nugroho, A. Sharma, S. Hultmark, A. I. Hofmann, R. Kroon, J. Benduhn, D.-M. Smilgies, K. Vandewal, M. R. Andersson, C. Langhammer, J. Martín, F. Gao, C. Müller, *ACS Appl. Mater. Interfaces.* **2019**, *11*, 21766.
[22] M. E. Farahat, M. A. Anderson, M. Martell, E. L. Ratcliff, G. C. Welch, *ACS Appl. Mater. Interfaces.* **2022**, *14*, 43558.

© 2024 The Author(s). Advanced Optical Materials published by Wiley-VCH GmbH

[23] A. G. Waketola, C. Pfukwa, P. Neethling, G. Bosman, Z. Genene, E. Wang, W. Mammo, F. G. Hone, N. A. Tegegne, *RSC Adv.* **2023**, *13*, 16175.
[24] A. G. Waketola, F. G. Hone, G. T. Mola, S. O. Oseni, H. Ogutu, N. A. Tegegne, *Appl. Phys. A* **2023**, *129*, 96.
[25] M. Knupfer, *Appl. Phys. A* **2003**, *77*, 623.
[26] J.-L. Brédas, J. E. Norton, J. Cornil, V. Coropceanu, *Acc. Chem. Res.* **2009**, *42*, 1691.
[27] C. Deibel, V. Dyakonov, *Reports Prog. Phys.* **2010**, *73*, 096401.
[28] L. J. A. Koster, V. D. Mihailetchi, H. Xie, P. W. M. Blom, *Appl. Phys. Lett.* **2005**, *87*, 203502.
[29] A. Wagenpfahl, D. Rauh, M. Binder, C. Deibel, V. Dyakonov, *Phys. Rev. B* **2010**, *82*, 115306.
[30] C. S. Lee, J. X. Tang, Y. C. Zhou, S. T. Lee, *Appl. Phys. Lett.* **2009**, *94*, 113304.
[31] I. T. Sachs-Quintana, T. Heumüller, W. R. Mateker, D. E. Orozco, R. Cheacharoen, S. Sweetnam, C. J. Brabec, M. D. McGehee, *Adv. Funct. Mater.* **2014**, *24*, 3978.
[32] M. Jørgensen, K. Norrman, F. C. Krebs, *Energy Mater. Sol. Cells* **2008**, *92*, 686.
[33] T. Oyamada, C. Maeda, H. Sasabe, C. Adachi, *Jpn. J. Appl. Phys.* **2003**, *42*, L1535.
[34] K. W. Wong, H. Yip, Y. Luo, K. Wong, W. Lau, K. Low, H. Chow, Z. Gao, W. Yeung, C. Chang, *Appl. Phys. Lett.* **2002**, *80*, 2788.
[35] A. W. Hains, T. J. Marks, *Appl. Phys. Lett.* **2008**, *92*, 023504.
[36] M. P. De Jong, L. J. Van Ijzendoorn, M. J. A. De Voigt, *Appl. Phys. Lett.* **2000**, *77*, 2255.
[37] M. S. White, D. C. Olson, S. E. Shaheen, N. Kopidakis, D. S. Ginley, *Appl. Phys. Lett.* **2006**, *89*, 143517.
[38] S. Anjusree, K. Arya, B. C. Das, *RSC Adv.* **2020**, *10*, 24882.
[39] Q. Bao, X. Liu, S. Braun, M. Fahlman, *Adv. Energy Mater.* **2014**, *4*, 1301272.
[40] C. Wang, S. Ni, S. Braun, M. Fahlman, X. Liu, *J. Mater. Chem. C* **2019**, *7*, 879.
[41] D. Fluhr, S. Züfle, B. Muhsin, R. Öttking, M. Seeland, R. Roesch, U. S. Schubert, B. Ruhstaller, S. Krischok, H. Hoppe, *Phys. Status Solidi A* **2018**, *215*, 1800474.
[42] A. Tournebize, D. Deribew, A. Gregori, R. C. Hiorns, A. Distler, H.-J. Egelhaaf, C. Lartigau-Dagron, A. Allal, A. Rivaton, H. Peisert, T. Chassé, *Sol. Energy Mater. Sol. Cells* **2019**, *200*, 110008.
[43] E. Voroshazi, B. Verreet, A. Buri, R. Müller, D. Di Nuzzo, P. Heremans, *Org. Electron.* **2011**, *12*, 736.
[44] J. Adams, M. Salvador, L. Lucera, S. Langner, G. D. Spyropoulos, F. W. Fecher, M. M. Voigt, S. A. Dowland, A. Osvet, H.-J. Egelhaaf, C. J. Brabec, *Adv. Energy Mater.* **2015**, *5*, 1501065.
[45] C. T. Howells, S. Saylan, H. Kim, K. Marbou, T. Aoyama, A. Nakao, M. Uchiyama, I. D. Samuel, D.-W. Kim, M. S. Dahlem, P. André, *J. Mater. Chem.* **2018**, *6*, 16012.
[46] C.-T. Lin, C.-T. Hsieh, T. J. Macdonald, J.-F. Chang, P.-C. Lin, H. Cha, L. Steier, A. Wadsworth, I. McCulloch, C.-C. Chueh, J. R. Durrant, *Adv. Funct. Mater.* **2022**, *32*, 2203487.
[47] V. N. Peters, M. O. Faruk, J. Asane, R. Alexander, A. P. D'angelo, S. Prayakarao, S. Rout, M. Noginov, *Optica* **2019**, *6*, 318.
[48] J. Schafferhans, A. Baumann, A. Wagenpfahl, C. Deibel, V. Dyakonov, *Org. Electron.* **2010**, *11*, 1693.
[49] A. Seemann, T. Sauermann, C. Lungenschmied, O. Armbruster, S. Bauer, H. J. Egelhaaf, J. Hauch, *Sol. Energy* **2011**, *85*, 1238.
[50] J. Razzell-Hollis, J. Wade, W. C. Tsoi, Y. Soon, J. Durrant, J. S. Kim, *J. Mater. Chem. A* **2014**, *2*, 20189.
[51] M. O. Reese, A. M. Nardes, B. L. Rupert, R. E. Larsen, D. C. Olson, M. T. Lloyd, S. E. Shaheen, D. S. Ginley, G. Rumbles, N. Kopidakis, *Adv. Funct. Mater.* **2010**, *20*, 3476.
[52] I. F. Domínguez, P. D. Topham, P. O. Bussiére, D. Bégué, A. Rivaton, *J. Phys. Chem. C* **2015**, *119*, 2166.
[53] R. H. Doremus, in *Reactivity of Solids*, (Eds.: J. W. Mitchell, R. C. DeVries, R. W. Roberts, P. Cannon) pp. 667–673. Wiley, New York **1969**.
[54] R. H. Doremus, *Diffusion of Reactive Molecules in Solids and Melts*, John Wiley & Sons, New York **2002**.
[55] J. Li, S. Kim, S. Edington, J. Nedy, S. Cho, K. Lee, A. J. Heeger, M. C. Gupta, J. T. Yates, *Sol. Energy Mater. Sol. Cells* **2011**, *95*, 1123.
[56] F. C. Krebs, K. Norrman, *Prog. Photovoltaics Res. Appl.* **2007**, *15*, 697.
[57] M. Salvador, N. Gasparini, J. D. Perea, S. H. Paleti, A. Distler, L. N. Inasaridze, P. Troshin, L. Lüer, H.-J. Egelhaaf, C. J. Brabec, *Energy Environ. Sci.* **2017**, *10*, 2005.
[58] A. V. Kesavan, K. K. Khanum, S. Subbiahraj, P. C. Ramamurthy, *J. Phys. Chem. C* **2019**, *123*, 22699.
[59] C. H. Peters, I. Sachs-Quintana, W. R. Mateker, T. Heumueller, J. Rivnay, R. Noriega, Z. M. Beiley, E. T. Hoke, A. Salleo, M. D. McGehee, *Adv. Mater.* **2012**, *24*, 663.
[60] N. Li, J. D. Perea, T. Kassar, M. Richter, T. Heumueller, G. J. Matt, Y. Hou, N. S. Güldal, H. Chen, S. Chen, S. Langner, M. Berlinghof, T. Unruh, C. J. Brabec, *Nat. Commun.* **2017**, *8*, 14541.
[61] M. N. Uvarov, M. S. Plekhanov, V. A. Zinoviev, V. V. Yanshole, M. V. Fedin, L. V. Kulik, *Chem. Phys. Lett.* **2020**, *754*, 137647.
[62] Y. W. Soon, S. Shoaee, R. S. Ashraf, H. Bronstein, B. C. Schroeder, W. Zhang, Z. Fei, M. Heeney, I. McCulloch, J. R. Durrant, *Adv. Funct. Mater.* **2014**, *24*, 1474.
[63] E. M. Speller, J. D. McGettrick, B. Rice, A. M. Telford, H. K. H. Lee, C.-H. Tan, C. S. De Castro, M. L. Davies, T. M. Watson, J. Nelson, J. R. Durrant, Z. Li, W. C. Tsoi, *ACS Appl. Mater. Interfaces.* **2017**, *9*, 22739.
[64] A. Nyga, A. Blacha-Grzechnik, P. Podsiadły, A. Duda, K. Kepska, M. Krzywiecki, R. Motyka, R. A. Janssen, P. Data, *Mater. Adv.* **2022**, *3*, 2063.
[65] E. L. Clennan, *Photochem. Photobiol.* **2023**, *99*, 204.
[66] N. Sai, K. Leung, J. Zádor, G. Henkelman, *Phys. Chem. Chem. Phys.* **2014**, *16*, 8092.
[67] M. Bregnhøj, M. Prete, V. Turkovic, A. U. Petersen, M. B. Nielsen, M. Madsen, P. R. Ogilby, *Methods Appl. Fluoresc.* **2019**, *8*, 014001.
[68] M. Prete, E. Ogliani, M. Bregnhøj, J. S. Lissau, S. Dastidar, H.-G. Rubahn, S. Engmann, A. L. Skov, M. A. Brook, P. R. Ogilby, A. Printz, V. Turkovic, M. Madsen, *J. Mater. Chem. C* **2021**, *9*, 11838.
[69] J. Guo, Y. Wu, R. Sun, W. Wang, J. Guo, Q. Wu, X. Tang, C. Sun, Z. Luo, K. Chang, Z. Zhang, J. Yuan, T. Li, W. Tang, E. Zhou, Z. Xiao, L. Ding, Y. Zou, X. Zhan, C. Yang, Z. Li, C. J. Brabec, Y. Li, J. Min, *J. Mater. Chem. A* **2019**, *7*, 25088.
[70] M. Manceau, S. Chambon, A. Rivaton, J.-L. Gardette, S. Guillerez, N. Lemaître, *Sol. Energy Mater. Sol. Cells* **2010**, *94*, 1572.
[71] A. Weu, J. A. Kress, F. Paulus, D. Becker-Koch, V. Lami, A. A. Bakulin, Y. Vaynzof, *ACS Appl. Energy Mater.* **2019**, *2*, 1943.
[72] Y. Wang, J. Luke, A. Privitera, N. Rolland, C. Labanti, G. Londi, V. Lemaur, D. T. W. Toolan, A. J. Sneyd, S. Jeong, D. Qian, Y. Olivier, L. Sorace, J.-S. Kim, D. Beljonne, Z. Li, A. J. Gillett, *Joule* **2023**, *7*, 810.
[73] S. Holliday, C. K. Luscombe, *Adv. Electron. Mater.* **2018**, *4*, 1700416.
[74] A. Tournebize, P.-O. Bussiére, P. Wong-Wah-Chung, S. Thérias, A. Rivaton, J.-L. Gardette, S. Beaupré, M. Leclerc, *Adv. Energy Mater.* **2013**, *3*, 478.
[75] G. Grause, M.-F. Chien, C. Inoue, *Polym. Degrad. Stab.* **2020**, *181*, 109364.
[76] M. Saito, I. Osaka, *J. Mater. Chem. C* **2018**, *6*, 3668.
[77] Y. Xin, G. Zeng, J. OuYang, X. Zhao, X. Yang, *J. Mater. Chem. C* **2019**, *7*, 9513.
[78] H. C. Wong, Z. . Li, C. H. Tan, H. Zhong, Z. Huang, H. Bronstein, I. McCulloch, J. T. Cabral, J. R. Durrant, *ACS Nano* **2014**, *8*, 1297.
[79] P. Li, M. Mainville, Y. Zhang, M. Leclerc, B. Sun, R. Izquierdo, D. Ma, *Small* **2019**, *15*, 1804671.

© 2024 The Author(s). Advanced Optical Materials published by Wiley-VCH GmbH

[80] J. Han, F. Bao, D. Huang, X. Wang, C. Yang, R. Yang, X. Jian, J. Wang, X. Bao, J. Chu, *Adv. Funct. Mater.* **2020**, *30*, 2003654.
[81] Z. Liu, N. Wang, *Nanoscale* **2018**, *10*, 19524.
[82] M. Campoy-Quiles, T. Ferenczi, T. Agostinelli, P. G. Etchegoin, Y. Kim, T. D. Anthopoulos, P. N. Stavrinou, D. D. C. Bradley, J. Nelson, *Nat. Mater* **2008**, *7*, 158.
[83] X. Yang, J. K. J. Van Duren, R. A. J. Janssen, M. A. J. Michels, J. Loos, *Macromolecules* **2004**, *37*, 2151.
[84] D. E. Motaung, G. F. Malgas, S. S. Nkosi, G. H. Mhlongo, B. W. Mwakikunga, T. Malwela, C. J. Arendse, T. F. G. Muller, F. Cumming, *J. Mater. Sci.* **2011**, *46*, 1763.
[85] N. Grossiord, J. M. Kroon, R. Andriessen, P. W. M. Blom, *Org. Electron.* **2012**, *13*, 432.
[86] M. Steinberger, A. Distler, C. J. Brabec, H.-J. Egelhaaf, *J. Phys. Chem. C* **2021**, *126*, 22.
[87] G.-U. Kim, Y. W. Lee, B. S. Ma, J. Kim, J. S. Park, S. Lee, T. L. Nguyen, M. Song, T.-S. Kim, H. Y. Woo, B. J. Kim, *J. Mater. Chem. A.* **2020**, *8*, 13522.
[88] Z. Wang, Z. Wang, Z. Wang, M. Zhao, Y. Zhou, B. Zhao, Y. Miao, P. Liu, Y. Hao, H. Wang, B. Xu, Y. Wu, S. Yin, *2D Mater.* **2019**, *6*, 045017.
[89] J.-W. Lee, C. Sun, D. J. Kim, M. Y. Ha, D. Han, J. S. Park, C. Wang, W. B. Lee, S.-K. Kwon, T.-S. Kim, Y.-H. Kim, B. J. Kim, *ACS nano* **2021**, *15*, 19970.
[90] C. Yan, J. Qin, Y. Wang, G. Li, P. Cheng, *Adv. Energy Mater.* **2022**, *12*, 2201087.
[91] W. R. Mateker, M. D. McGehee, *Adv. Mater.* **2017**, *29*, 1603940.
[92] L. Ye, B. A. Collins, X. Jiao, J. Zhao, H. Yan, H. Ade, *Adv. Energy Mater.* **2018**, *8*, 1703058.
[93] K. An, W. Zhong, F. Peng, W. Deng, Y. Shang, H. Quan, H. Qiu, C. Wang, F. Liu, H. Wu, N. Li, F. Huang, L. Ying, *Nat. Commun.* **2023**, *14*, 2688.
[94] W. You, D. Zhou, L. Hu, H. Xu, Y. Tong, B. Hu, Y. Xie, Z. Li, M. Li, L. Chen, *Solar RRL* **2021**, *5*, 2100532.
[95] Y. Cai, Q. Li, G. Lu, H. S. Ryu, Y. Li, H. Jin, Z. Chen, Z. Tang, G. Lu, X. Hao, H. Y. Woo, C. Zhang, Y. Sun, *Nat. Commun.* **2022**, *13*, 2369.
[96] D. He, J. Zhou, Y. Zhu, Y. Li, K. Wang, J. Li, J. Zhang, B. Li, Y. Lin, Y. He, C. Wang, F. Zhao, *Adv. Mater.* **2024**, *36*, 2308909.
[97] M. Kim, J. Lee, S. B. Jo, D. H. Sin, H. Ko, H. Lee, S. G. Lee, K. Cho, *J. Mater. Chem. A* **2016**, *4*, 15522.
[98] C. Caddeo, J. Ackermann, A. Mattoni, *Solar RRL* **2022**, *6*, 2200172.
[99] L. Duan, Y. Zhang, M. He, R. Deng, H. Yi, Q. Wei, Y. Zou, A. Uddin, *ACS Appl. Mater. Interfaces.* **2020**, *12*, 27433.
[100] S. Park, H. J. Son, *J. Mater. Chem. A* **2019**, *7*, 25830.
[101] X. Gu, X. Lai, Y. Zhang, T. Wang, W. L. Tan, C. R. McNeill, Q. Liu, P. Sonar, F. He, W. Li, C. Shan, A. K. K. Kyaw, *Adv. Sci.* **2022**, *9*, 2200445.
[102] J. Wang, Z. Zheng, P. Bi, Z. Chen, Y. Wang, X. Liu, S. Zhang, X. Hao, M. Zhang, Y. Li, J. Hou, *Natl. Sci. Rev.* **2023**, *10*, nwad085.
[103] Z.-X. Liu, Z.-P. Yu, Z. Shen, C. He, T.-K. Lau, Z. Chen, H. Zhu, X. Lu, Z. Xie, H. Chen, C.-Z. Li, *Nat. Commun.* **2021**, *12*, 3049.
[104] Y. Xin, G. Zeng, J. OuYang, X. Zhao, X. Yang, *J. Mater. Chem. C* **2019**, *7*, 9513.
[105] J. Zhang, Y. Han, W. Zhang, J. Ge, L. Xie, Z. Xia, W. Song, D. Yang, X. Zhang, Z. Ge, *ACS Appl. Mater. Interfaces.* **2020**, *12*, 57271.
[106] S.-C. Wu, L. T. Strover, X. Yao, X.-Q. Chen, W.-J. Xiao, L.-N. Liu, J. Wang, I. Fisher-Visoly, E. A. Katz, W.-S. Li, *Appl. Mater. Interfaces* **2018**, *10*, 35430.
[107] J. Lee, J.-H. Lee, H. Yao, H. Cha, S. Hong, S. Lee, J. Kim, J. R. Durrant, J. Hou, K. Lee, *J. Mater. Chem. A* **2020**, *8*, 6682.
[108] C. Zhang, A. Mumyatov, S. Langner, J. D. Perea, T. Kassar, J. Min, L. Ke, H. Chen, K. L. Gerasimov, D. V. Anokhin, D. A. Ivanov, T. Ameri, A. Osvet, D. K. Susarova, T. Unruh, N. Li, P. Troshin, C. Brabec, *Adv. Energy Mater.* **2017**, *7*, 1601204.
[109] N. Bauer, Q. Zhang, J. Zhao, L. Ye, J.-H. Kim, I. Constantinou, L. Yan, F. So, H. Ade, H. Yan, W. You, *J. Mater. Chem. A.* **2017**, *5*, 4886.
[110] T. Kim, J. Choi, H. J. Kim, W. Lee, B. J. Kim, *Macromolecules* **2017**, *50*, 6861.
[111] T. Heumueller, W. R. Mateker, A. Distler, U. F. Fritze, R. Cheacharoen, W. H. Nguyen, M. Biele, M. Salvador, M. von Delius, H.-J. Egelhaaf, M. D. McGehee, C. J. Brabec, *Energy Environ. Sci.* **2016**, *9*, 247.
[112] Y. Bai, X. Yao, J. Wang, J.-L. Wang, S.-C. Wu, S.-P. Yang, W.-S. Li, *Tetrahedron* **2019**, *75*, 4676.
[113] J. W. Rumer, I. McCulloch, *Mater. Today* **2015**, *18*, 425.
[114] M.-H. Liao, C.-E. Tsai, Y.-Y. Lai, F.-Y. Cao, J.-S. Wu, C.-L. Wang, C.-S. Hsu, I. Liau, Y.-J. Cheng, *Adv. Funct. Mater.* **2014**, *24*, 1418.
[115] J. Wang, Y. Xie, K. Chen, H. Wu, J. M. Hodgkiss, X. Zhan, *Nat. Rev. Phys.* **2024**, *6*, 365.
[116] P. Cheng, X. Zhan, *Chem. Soc. Rev.* **2016**, *45*, 2544.
[117] X. Du, T. Heumueller, W. Gruber, O. Almora, A. Classen, J. Qu, F. He, T. Unruh, N. Li, C. J. Brabec, *Adv. Mater.* **2020**, *32*, 1908305.
[118] C. Labanti, M. J. Sung, J. Luke, S. Kwon, R. Kumar, J. Hong, J. Kim, A. A. Bakulin, S.-K. Kwon, Y.-H. Kim, J.-S. Kim, *Acs Nano* **2021**, *15*, 7700.
[119] P. Cheng, G. Li, X. Zhan, Y. Yang, *Nat. Photonics* **2018**, *12*, 131.
[120] C. Yan, S. Barlow, Z. Wang, H. Yan, A. K.-Y. Jen, S. R. Marder, X. Zhan, *Nat. Rev. Mater.* **2018**, *3*, 18003.
[121] J. Wang, P. Xue, Y. Jiang, Y. Huo, X. Zhan, *Nat. Rev. Chem.* **2022**, *6*, 614.
[122] Y. Lin, F. Zhao, Q. He, L. Huo, Y. Wu, T. C. Parker, W. Ma, Y. Sun, C. Wang, D. Zhu, A. J. Heeger, S. R. Marder, X. Zhan, *J. Am. Chem. Soc.* **2016**, *138*, 4955.
[123] C. Labanti, M. J. Sung, J. Luke, S. Kwon, R. Kumar, J. Hong, J. Kim, A. A. Bakulin, S.-K. Kwon, Y.-H. Kim, J.-S. Kim, *ACS Nano* **2021**, *15*, 7700.
[124] X. Liu, C. Zhang, S. Pang, N. Li, C. J. Brabec, C. Duan, F. Huang, Y. Cao, *Front. Chem.* **2020**, *8*, 302.
[125] A. J. Clarke, J. Luke, R. Meitzner, J. Wu, Y. Wang, H. K. Lee, E. M. Speller, H. Bristow, H. Cha, M. J. Newman, K. Hooper, A. Evans, F. Gao, H. Hoppe, I. McCulloch, U. S. Schubert, T. M. Watson, J. R. Durrant, W. C. Tsoi, J.-S. Kim, Z. Li, *Cell Rep. Phys. Sci.* **2021**, *2*, 100498.
[126] V. Vohra, Y. Matsunaga, T. Takada, A. Kiyokawa, L. Barba, W. Porzio, *Small* **2021**, *17*, 2004168.
[127] L. Zhang, H. Zhao, M. Hu, X. Wang, L. Hu, H. Mao, Z. Yuan, W. Ma, Y. Chen, *Small* **2021**, *17*, 2103537.
[128] Z. Liu, N. Wang, *Nanoscale* **2018**, *10*, 19524.
[129] W. Yang, Z. Luo, R. Sun, J. Guo, T. Wang, Y. Wu, W. Wang, J. Guo, Q. Wu, M. Shi, H. Li, C. Yang, J. Min, *Nat. Commun.* **2020**, *11*, 1218.
[130] L. Zhang, H. Zhao, J. Yuan, B. Lin, Z. Xing, X. Meng, L. Ke, X. Hu, W. Ma, Y. Yuan, *Org. Electron.* **2020**, *83*, 105771.
[131] Y. Zhang, Y. Xu, M. J. Ford, F. Li, J. Sun, X. Ling, Y. Wang, J. Gu, J. Yuan, W. Ma, *Adv. Energy Mater.* **2018**, *8*, 1800029.
[132] N. Gasparini, S. H. K. Paleti, J. Bertrandie, G. Cai, G. Zhang, A. Wadsworth, X. Lu, H.-L. Yip, I. McCulloch, D. Baran, *ACS Energy Lett.* **2020**, *5*, 1371.
[133] M. Gunther, D. Blatte, A. L. Oechsle, S. S. Rivas, A. A. Yousefi Amin, P. Müller-Buschbaum, T. Bein, T. Ameri, *ACS Appl. Mater. Interfaces.* **2021**, *13*, 19072.
[134] A. Distler, K.-S. Cheon, D. Waller, D. Guldi, J. Hauch, H.-J. Egelhaaf, *J. Mater. Chem. C* **2021**, *9*, 9271.
[135] E. M. Speller, A. J. Clarke, N. Aristidou, M. F. Wyatt, L. Francàs, G. Fish, H. Cha, H. K. H. Lee, J. Luke, A. Wadsworth, A. D. Evans, I. McCulloch, J.-S. Kim, S. A. Haque, J. R. Durrant, S. D. Dimitrov, W. C. Tsoi, Z. Li, *ACS Energy Lett.* **2019**, *4*, 846.
[136] I. V. Martynov, L. N. Inasaridze, P. A. Troshin, *ChemSusChem* **2021**, *14*, 1.
[137] N. Y. Doumon, G. Wang, R. C. Chiechi, L. J. A. Koster, *J. Mater. Chem. C* **2017**, *5*, 6611.

© 2024 The Author(s). Advanced Optical Materials published by Wiley-VCH GmbH

[138] N. Y. Doumon, G. Wang, X. Qiu, A. J. Minnaard, R. C. Chiechi, L. J. A. Koster, *Sci. Rep.* **2019**, *9*, 1.
[139] B. S. Desalegn, N. Bekri, F. G. Hone, D. M. Andoshe, W. Mammo, Z. Abdissa, G. Bosman, N. A. Tegegne, *Mater. Today Commun.* **2021**, *29*, 102803.
[140] C. Zhang, A. Song, Q. Huang, Y. Cao, Z. Zhong, Y. Liang, K. Zhang, C. Liu, F. Huang, Y. Cao, *Nanomicro Lett.* **2023**, *15*, 140.
[141] J. Min, C. Cui, T. Heumueller, S. Fladischer, X. Cheng, E. Spiecker, Y. Li, C. J. Brabec, *Adv. Energy Mater.* **2016**, *6*, 1600515.
[142] H. Chen, Z. Hu, H. Wang, L. Liu, P. Chao, J. Qu, W. Chen, A. Liu, F. He, *Joule* **2018**, *2*, 1623.
[143] N. Y. Doumon, L. J. A. Koster, *Sol. RRL* **2019**, *3*, 1800301.
[144] F.-J. Kahle, C. Saller, A. Köhler, P. Strohriegl, *Adv. Energy Mater.* **2017**, *7*, 1700306.
[145] F. Yang, W. Zhao, Q. Zhu, C. Li, W. Ma, J. Hou, W. Li, *Macromolecules* **2019**, *52*, 2214.
[146] W. Feng, Z. Lin, J. Cui, W. Lv, W. Wang, Q. Ling, *Sol. Energy Mater. Sol. Cells* **2019**, *200*, 109982.
[147] X. Yi, C. H. Y. Ho, B. Gautam, L. Lei, A. H. Chowdhury, B. Bahrami, Q. Qiao, F. So, *J. Mater. Chem. C* **2020**, *8*, 16092.
[148] H. Cao, W. He, Y. Mao, X. Lin, K. Ishikawa, J. H. Dickerson, W. P. Hess, *J. Power Sources* **2014**, *264*, 168.
[149] D. Hashemi, X. Ma, R. Ansari, J. Kim, J. Kieffer, *Phys. Chem. Chem. Phys.* **2019**, *21*, 789.
[150] Q. Zhao, J. Qu, F. He, *Adv. Sci.* **2020**, *7*, 2000509.
[151] J. Shin, M. Kim, B. Kang, J. Lee, H. G. Kim, K. Cho, *J. Mater. Chem. A* **2017**, *5*, 16702.
[152] D. Deng, Y. Zhang, J. Zhang, Z. Wang, L. Zhu, J. Fang, B. Xia, Z. Wang, K. Lu, W. Ma, Z. Wei, *Nat. Commun.* **2016**, *7*, 13740.
[153] V. N. Viswanathan, A. J. Ferguson, J. R. Pfeilsticker, B. W. Larson, L. E. Garner, C. P. Brook, S. H. Strauss, O. V. Boltalina, P. C. Ramamurthy, W. A. Braunecker, *Org. Electron.* **2018**, *62*, 685.
[154] L. Lu, T. Zheng, Q. Wu, A. M. Schneider, D. Zhao, L. Yu, *Chem. Rev.* **2015**, *115*, 12666.
[155] R. Hu, Y. Liu, L. Zhang, W. Xiao, W. Zhang, *Chem. Phys.* **2023**, *572*, 111965.
[156] Y. Ge, L. Hu, L. Zhang, Q. Fu, G. Xu, Z. Xing, L. Huang, W. Zhou, Y. Chen, *ACS Appl. Mater. Interfaces.* **2020**, *12*, 10706.
[157] L.-Y. Su, H.-H. Huang, Y.-C. Lin, G.-L. Chen, W.-C. Chen, W. Chen, L. Wang, C.-C. Chueh, *Adv. Funct. Mater.* **2021**, *31*, 2005753.
[158] Q. Zhou, C. Yan, H. Li, Z. Zhu, Y. Gao, J. Xiong, H. Tang, C. Zhu, H. Yu, S. P. G. Lopez, J. Wang, M. Qin, J. Li, L. Luo, X. Liu, J. Qin, S. Lu, L. Meng, F. Laquai, Y. Li, P. Cheng, *Nanomicro Lett.* **2024**, *16*, 224.
[159] P. Cheng, C. Yan, T.-K. Lau, J. Mai, X. Lu, X. Zhan, *Adv. Mater.* **2016**, *28*, 5822.
[160] X. Du, Y. Yuan, L. Zhou, H. Lin, C. Zheng, J. Luo, Z. Chen, S. Tao, L.-S. Liao, *Adv. Funct. Mater.* **2020**, *30*, 1909837.
[161] B. Liu, H. Sun, J.-W. Lee, Z. Jiang, J. Qiao, J. Wang, J. Yang, K. Feng, Q. Liao, M. An, B. Li, D. Han, B. Xu, H. Lian, L. Niu, B. J. Kim, X. Guo, *Nat. Commun.* **2023**, *14*, 967.
[162] Y. Cheng, B. Huang, Q. Mao, X. Huang, J. Liu, C. Zhou, W. Zhou, X. Ren, S. Kim, W. Kim, Z. Sun, F. Wu, C. Yang, L. Chen, *Adv. Mater.* **2024**, *36*, 2312938.
[163] S. Braun, W. R. Salaneck, M. Fahlman, *Adv. Mater.* **2009**, *21*, 1450.
[164] J. H. Kang, J. H. Lee, B. Walker, J. H. Seo, G. S. Chang, *J. Appl. Phys.* **2022**, *132*, 050701.
[165] Z. Zheng, R. Wang, H. Yao, S. Xie, Y. Zhang, J. Hou, H. Zhou, Z. Tang, *Nano Energy* **2018**, *50*, 169.
[166] Y. Ge, L. Hu, L. Zhang, Q. Fu, G. Xu, Z. Xing, L. Huang, W. Zhou, Y. Chen, *ACS Appl. Mater. Interfaces.* **2020**, *12*, 10706.
[167] C. Zhu, X. Wang, W. Liu, Y. Liu, X. Zhan, *Trends Chem.* **2024**, *6*, 37.
[168] Y. Zhang, M. Li, J. Fang, D. Xia, S. You, C. Zhao, J. Zhang, W. Li, *Sustain. Energy Fuels.* **2022**, *6*, 4115.
[169] Z. Yin, J. Wei, Q. Zheng, *Adv. Sci.* **2016**, *3*, 1500362.
[170] G. Sherafatipour, J. Benduhn, B. R. Patil, M. Ahmadpour, D. Spoltore, H.-G. Rubahn, K. Vandewal, M. Madsen, *Sci. Rep.* **2019**, *9*, 4024.
[171] K. G. Gebremariam, F. G. Hone, J. Dai, G. T. Mola, W. Mammo, N. A. Tegegne, *New J. Chem.* **2023**, *47*, 13331.
[172] B. A. MacLeod, B. J. T. De Villers, P. Schulz, P. F. Ndione, H. Kim, A. J. Giordano, K. Zhu, S. R. Marder, S. Graham, J. J. Berry, A. Kahn, D. C. Olson, *Energy Environ. Sci.* **2015**, *8*, 592.
[173] A. Soultati, A. Verykios, T. Speliotis, M. Fakis, I. Sakellis, H. Jaouani, D. Davazoglou, P. Argitis, M. Vasilopoulou, *Org. Electron.* **2019**, *71*, 227.
[174] L. Yan, Y. Wang, W. Zhao, H. Zha, H. Song, H. Hao, Y. Hao, Q. Luo, F. Liu, Y. Yang, Q. Su, H. Wang, C.-Q. Ma, *Cell Rep. Phys. Sci.* **2023**, *4*, 101654.
[175] S. K. Swami, J. I. Khan, V. Dutta, J. Lee, F. Laquai, N. Chaturvedi, *ACS Appl. Energy Mater.* **2023**, *6*, 2906.
[176] J. Luo, Z. Feng, X. Liu, Z. Li, *IEEE J. Photovolt.* **2021**, *11*, 374.
[177] J. Wang, H. Pan, X. Xu, H. Jin, W. Ma, S. Xiong, Q. Bao, Z. Tang, Z. Ma, *ACS Appl. Mater. Interfaces.* **2022**, *14*, 12450.
[178] E. Moustafa, J. G. Sanchez, L. F. Marsal, J. Pallarès, *ACS Appl. Energy Mater.* **2021**, *4*, 4099.
[179] D. Günther, M. Blätte, A. L. Oechsle, S. S. Rivas, A. A. Yousefi Amin, P. Müller-Buschbaum, T. Bein, T. Ameri, *ACS Appl. Mater. Interfaces* **2021**, *13*, 19072.
[180] M. Nakano, S. Nakagawa, F. Sato, M. Shahiduzzaman, M. Karakawa, T. Taima, K. Takahashi, *ACS Appl. Energy Mater.* **2021**, *4*, 6385.
[181] K. G. Gebremariam, F. G. Hone, A. Negash, Z. Genene, J. Dai, A. G. Waketola, G. T. Mola, W. Mammo, N. A. Tegegne, *Energy Fuels* **2024**, *38*, 3304.
[182] M. Sadeghianlemraski, B. Y. Lee, T. Davidson-Hall, Z. Leonenko, H. Aziz, *Org. Electron.* **2019**, *73*, 26.
[183] M. Li, W. Zha, Y. Han, B. Liu, Q. Luo, C.-Q. Ma, *Org. Electron.* **2021**, *96*, 106257.
[184] J. Wei, C. Zhang, G. Ji, Y. Han, I. Ismail, H. Li, Q. Luo, J. Yang, C.-Q. Ma, *J. Sol. Energy* **2019**, *193*, 102.
[185] G. K. Dalapati, H. Sharma, A. Guchhait, N. Chakrabarty, P. Bamola, Q. Liu, G. Saianand, A. M. S. Krishna, S. Mukhopadhyay, A. Dey, T. K. Shun Wong, S. Zhuk, S. Ghosh, S. Chakrabortty, C. Mahata, S. Biring, A. Kumar, C. S. Ribeiro, S. Ramakrishna, A. K. Chakraborty, S. Krishnamurthy, P. Sonar, M. Sharma, *J. Mater. Chem. A* **2021**, *9*, 16621.
[186] L. Di Mario, D. Garcia Romero, H. Wang, E. K. Tekelenburg, S. Meems, T. Zaharia, G. Portale, M. A. Loi, *Adv. Mater.* **2023**, 2301404.
[187] A. V. Keskin, M. Gençten, S. Bozar, M. B. Arvas, S. Güneş, Y. Sahin, *Thin Solid Films* **2020**, *706*, 138093.
[188] M. Vasilopoulou, N. Kelaidis, E. Polydorou, A. Soultati, D. Davazoglou, P. Argitis, G. Papadimitropoulos, D. Tsikritzis, S. Kennou, F. Auras, D. G. Georgiadou, S.-R. G. Christopoulos, A. Chroneos, *Sci. Rep.* **2017**, *7*, 17839.
[189] D. Li, Y. Chen, P. Du, Z. Zhao, H. Zhao, Y. Ma, Z. Sun, *RSC Adv.* **2015**, *5*, 88973.
[190] Y.-C. Tu, J.-F. Lin, W.-C. Lin, C.-P. Liu, J.-J. Shyue, W.-F. Su, *Cryst. Eng. Comm.* **2012**, *14*, 4772.
[191] K. Park, J.-H. Kim, J. S. Jin, H. Moon, J. Oh, S. Lee, T. Ki, H.-S. Jeong, S. Jeong, S.-Y. Jang, H. Kang, K. Lee, *ACS Appl. Mater. Interfaces.* **2024**, *16*, 3778.
[192] Z. Yin, S. Mei, P. Gu, H.-Q. Wang, W. Song, *iScience* **2021**, *24*, 103027.
[193] F.-C. Hsu, Y.-A. Lin, C.-P. Li, *Org. Electron.* **2021**, *89*, 106008.
[194] Y. Cui, H. Yao, L. Hong, T. Zhang, Y. Tang, B. Lin, K. Xian, B. Gao, C. An, P. Bi, W. Ma, J. Hou, *Natl. Sci. Rev.* **2020**, *7*, 1239.
[195] H. Bin, J. Wang, J. Li, M. M. Wienk, R. A. Janssen, *Adv. Mater.* **2021**, *33*, 2008429.

© 2024 The Author(s). Advanced Optical Materials published by Wiley-VCH GmbH

[196] F. Hermerschmidt, A. Savva, E. Georgiou, S. M. Tuladhar, J. R. Durrant, I. McCulloch, D. D. Bradley, C. J. Brabec, J. Nelson, S. A. Choulis, *ACS Appl. Mater. Interfaces.* **2017**, *9*, 14136.
[197] X. Hu, L. Chen, Y. Chen, *J. Phys. Chem. C* **2014**, *118*, 9930.
[198] S. Wu, S. Han, Y. Zheng, H. Zheng, N. Liu, L. Wang, Y. Cao, J. Wang, *Org. Electron.* **2011**, *12*, 504.
[199] D. Akın Kara, K. Kara, G. Oylumluoglu, M. Z. Yigit, M. Can, J. J. Kim, E. K. Burnett, D. L. Gonzalez Arellano, S. Buyukcelebi, F. Ozel, O. Usluer, A. L. Briseno, M. Kus, *ACS Appl. Mater. Interfaces.* **2018**, *10*, 30000.
[200] H. Shen, T. Hu, H. Huang, D. Wu, J. Xia, *J. Mater. Sci.: Mater. Electron.* **2022**, *33*, 12083.
[201] B. Xu, S.-A. Gopalan, A.-I. Gopalan, N. Muthuchamy, K.-P. Lee, J.-S. Lee, Y. Jiang, S.-W. Lee, S.-W. Kim, J.-S. Kim, H.-M. Jeong, J.-B. Kwon, J.-H. Bae, S.-W. Kang, *Sci. Rep.* **2017**, *7*, 45079.
[202] B. V. R. S. Subramanyam, P. C. Mahakul, K. Sa, J. Raiguru, I. Alam, S. Das, M. Mondal, S. Subudhi, P. Mahanandia, *Sol. Energy* **2019**, *186*, 146.
[203] B. Subramanyam, P. C. Mahakul, K. Sa, J. Raiguru, P. Mahanandia, *J. Phys: Mater.* **2020**, *3*, 045004.
[204] S. Rafique, S. M. Abdullah, W. E. Mahmoud, A. A. Al-Ghamdi, K. Sulaiman, *RSC Adv.* **2016**, *6*, 50043.
[205] F. Cheng, Y. Wu, Y. Shen, X. Cai, L. Li, *RSC Adv.* **2017**, *7*, 37952.
[206] C. Albonetti, V. El Qacemi, S. Limage, C. Versini, L.-D. Kauffmann, M. Muccini, M. Seri, *Phys. Status Solidi A* **2021**, *218*, 2000748.
[207] M. Y. Ameen, P. Shamjid, T. Abhijith, T. Radhakrishnan, V. Reddy, *Phys. B: Condens. Matter.* **2018**, *530*, 201.
[208] M. Y. Ameen, P. Shamjid, T. Abhijith, V. Reddy, *Opt. Mater.* **2018**, *75*, 491.
[209] W. Greenbank, N. Rolston, E. Destouesse, G. Wantz, L. Hirsch, R. Dauskardt, S. Chambon, *J. Mater. Chem. A* **2017**, *5*, 2911.
[210] Z. Jiang, F. Wang, K. Fukuda, A. Karki, W. Huang, K. Yu, T. Yokota, K. Tajima, T.-Q. Nguyen, T. Someya, *Proc. Natl. Acad. Sci.* **2020**, *117*, 6391.
[211] X. Wang, H. Jin, R. C. Nagiri, B. Z. Poliquit, J. Subbiah, D. J. Jones, N. Kopidakis, P. L. Burn, J. Yu, *Sol. RRL* **2019**, *3*, 1800286.
[212] T. F. O'Connor, A. V. Zaretski, S. Savagatrup, A. D. Printz, C. D. Wilkes, M. I. Diaz, E. J. Sawyer, D. J. Lipomi, *Sol. Energy Mater. Sol. Cells* **2016**, *144*, 438.
[213] D. Koo, S. Jung, J. Seo, G. Jeong, Y. Choi, J. Lee, S. M. Lee, Y. Cho, M. Jeong, J. Lee, J. Oh, C. Yang, H. Park, *Joule* **2020**, *4*, 1021.
[214] D. H. Shin, C. W. Jang, J. S. Ko, S.-H. Choi, *Appl. Surf. Sci.* **2021**, *538*, 148155.
[215] W. Zhang, W. Song, J. Huang, L. Huang, T. Yan, J. Ge, R. Peng, Z. Ge, *J. Mater. Chem. A* **2019**, *7*, 22021.
[216] Z. Liu, N. Wang, *J. Mater. Chem. C* **2018**, *6*, 9734.
[217] S. Wageh, M. Raïssi, T. Berthelot, M. Laurent, D. Rousseau, A. M. Abusorrah, O. A. Al-Hartomy, A. A. Al-Ghamdi, *Sci. Rep.* **2021**, *11*, 14212.
[218] M. O. Reese, S. A. Gevorgyan, M. Jorgensen, E. Bundgaard, S. R. Kurtz, D. S. Ginley, D. C. Olson, M. T. Lloyd, P. Morvillo, E. A. Katz, A. Elschner, O. Haillant, T. R. Currier, V. Shrotriya, M. Hermenau, M. Riede, K. R. Kirov, G. Trimmel, T. Rath, O. Inganäs, F. Zhang, M. Andersson, K. Tvingstedt, M. Lira-Cantu, D. Laird, C. McGuiness, S. Gowrisanker, M. Pannone, M. Xiao, J. Hauch, et al., *Sol. Energy Mater. Sol. Cells* **2011**, *95*, 1253.
[219] S. A. Gevorgyan, A. J. Medford, E. Bundgaard, S. B. Sapkota, H.-F. Schleiermacher, B. Zimmermann, U. Würfel, A. Chafiq, M. Lira-Cantu, T. Swonke, M. Wagner, C. J. Brabec, O. Haillant, E. Voroshazi, T. Aernouts, R. Steim, J. A. Hauch, A. Elschner, M. Pannone, M. Xiao, A. Langzettel, D. Laird, M. T. Lloyd, T. Rath, E. Maier, G. Trimmel, M. Hermenau, T. Menke, K. Leo, R. Rösch, et al., *Sol. Energy Mater. Sol. Cells* **2011**, *95*, 1398.
[220] M. V. Madsen, S. A. Gevorgyan, R. Pacios, J. Ajuria, I. Etxebarria, J. Kettle, N. D. Bristow, M. Neophytou, S. A. Choulis, L. S. Roman, T. Yohannes, A. Cester, P. Cheng, X. Zhan, J. Wu, Z. Xie, W.-C. Tu, J.-H. He, C. J. Fell, K. Anderson, M. Hermenau, D. Bartesaghi, L. J. A. Koster, F. Machui, I. González-Valls, M. Lira-Cantu, P. P. Khlyabich, B. C. Thompson, R. Gupta, K. Shanmugam, et al., *Sol. Energy Mater. Sol. Cells* **2014**, *130*, 281.
[221] D. M. Tanenbaum, M. Hermenau, E. Voroshazi, M. T. Lloyd, Y. Galagan, B. Zimmermann, M. Hösel, H. F. Dam, M. Jørgensen, S. A. Gevorgyan, S. Kudret, W. Maes, L. Lutsen, D. Vanderzande, U. Würfel, R. Andriessen, R. Rösch, H. Hoppe, G. Teran-Escobar, M. Lira-Cantu, A. Rivaton, G. Y. Uzunoğlu, D. Germack, B. Andreasen, M. V. Madsen, K. Norrman, F. C. Krebs, *RSC Adv.* **2012**, *2*, 882.
[222] O. Haillant, D. Dumbleton, A. Zielnik, *Sol. Energy Mater. Sol. Cells* **2011**, *95*, 1889.
[223] S.-C. Wu, L. T. Strover, X. Yao, X.-Q. Chen, W.-J. Xiao, L.-N. Liu, J. Wang, I. Visoly-Fisher, E. A. Katz, W. S. Li, *ACS Appl. Mater. Interfaces.* **2018**, *10*, 35430.
[224] W. Yang, Z. Luo, R. Sun, J. Guo, T. Wang, Y. Wu, W. Wang, J. Guo, Q. Wu, M. Shi, H. Li, Y. Chuluo, J. Min, *Nat. Commun.* **2020**, *11*, 1218.
[225] D. Lee, J. Kim, G. Park, H. W. Bae, M. An, J. Y. Kim, *Polymers* **2020**, *12*, 992.
[226] Z. Jiang, F. Wang, K. Fukuda, A. Karki, W. Huang, K. Yu, T. Yokota, K. Tajima, T.-Q. Nguyen, T. Someya, *Proc. Natl. Acad. Sci.* **2020**, *117*, 6391.
[227] Y. Xin, G. Zeng, J. OuYang, X. Zhao, *J. Mater. Chem. C* **2019**, *7*, 9513.
[228] A. A. Melvin, V. D. Stoichkov, J. Kettle, D. Mogilyansky, E. A. Katz, V.-F. Iris, *Sol. Energy* **2018**, *159*, 794.
[229] T. Leijtens, G. E. Eperon, S. Pathak, A. Abate, M. M. Lee, H. J. Snaith, *Nat. Commun.* **2013**, *4*, 2885.
[230] S. B. Sapkota, M. Fischer, B. Zimmermann, U. Wurfel, *Sol. Energy Mater. Sol. Cells* **2014**, *121*, 43.
[231] S. Venkatesan, E. Nho, D. Khatiwada, C. Zhang, Q. Qiao, *ACS Appl. Mater. Interfaces.* **2015**, *7*, 16093.
[232] J. Jeong, J. Seo, S. Nam, H. Han, H. Kim, T. D. Anthopoulos, D. D. C. Bradley, Y. Kim, *Adv. Sci.* **2016**, *3*, 1500269.
[233] T. Glen, N. Scarratt, H. Yi, A. Iraqi, T. Wang, J. Kingsley, A. Buckley, D. Lidzey, A. Donald, *Sol. Energy Mater. Sol. Cells* **2015**, *140*, 25.
[234] T. S. Glen, N. W. Scarratt, H. Yi, A. Iraqi, T. Wang, J. Kingsley, A. R. Buckley, D. G. Lidzey, A. M. Donald, *J. Polym. Sci., Part B: Polym. Phys.* **2016**, *54*, 216.
[235] X. Wang, C. X. Zhao, G. Xu, Z.-K. Chen, F. Zhu, *Sol. Energy Mater. Sol. Cells* **2012**, *104*, 1.
[236] X. Du, T. Heumueller, W. Gruber, A. Classen, T. Unruh, N. Li, C. J. Brabec, *Joule* **2019**, *3*, 215.
[237] Q. Burlingame, X. Huang, X. Liu, C. Jeong, C. Coburn, S. R. Forrest, *Nature* **2019**, *573*, 394.
[238] G. Sherafatipour, J. Benduhn, B. R. Patil, M. Ahmadpour, D. Spoltore, H. G. Rubahn, K. Vandewal, M. Madsen, *Sci. Rep.* **2019**, *9*, 1.
[239] P. Li, M. Mainville, Y. Zhang, M. Leclerc, B. Sun, R. Izquierdo, D. Ma, *Small* **2019**, *15*, 1.
[240] D. Lee, J. Kim, G. Park, H. W. Bae, M. An, J. Y. Kim, *Polymers* **2020**, *12*, 1.
[241] L. Duan, X. Meng, Y. Zhang, H. Yi, K. Jin, F. Haque, C. Xu, Z. Xiao, L. Ding, A. Uddin, *Mater. Chem. Front.* **2019**, *3*, 1085.
[242] F. F. Muhammad, K. Sulaiman, *ARO-The Scientific Journal of Koya University* **2018**, *4*, 69.
[243] Z. Jiang, F. Wang, K. Fukuda, A. Karki, W. Huang, K. Yu, T. Yokota, K. Tajima, T.-Q. Nguyen, T. Someya, *Proc. Natl. Acad. Sci.* **2020**, *117*, 6391.
[244] L. Duan, M. Guli, Y. Zhang, H. Yi, F. Haque, A. Uddin, *Energy Technol.* **2020**, *8*, 1901401.

© 2024 The Author(s). Advanced Optical Materials published by Wiley-VCH GmbH

[245] J. Xiao, M. Ren, G. Zhang, J. Wang, D. Zhang, L. Liu, N. Li, J. B. Christoph, H.-L. Yip, Y. Cao, *Sol. RRL* **2019**, *3*, 1900077.
[246] J. Zhang, Y. Han, W. Zhang, J. Ge, L. Xie, Z. Xia, W. Song, D. Yang, *Appl. Mater. Interfaces.* **2020**, *12*, 57271.
[247] L. Duan, Y. Zhang, M. He, R. Deng, H. Yi, Q. Wei, Y. Zou, A. Uddin, *Appl. Mater. Interfaces* **2020**, *12*, 27433.
[248] Y. Liang, D. Zhang, Z. Wu, T. Jia, L. Lüer, H. Tang, L. Hong, J. Zhang, K. Zhang, C. J. Brabec, N. Li, F. Huang, *Nat. Energy* **2022**, *7*, 1180.
[249] S. Tu, X. Lin, L. Xiao, H. Zhen, W. Wang, Q. Ling, *Mater. Chem. Front.* **2022**, *6*, 1150.
[250] Y. Zhao, Z. Wu, X. Liu, Z. Zhong, R. Zhu, J. Yu, *J. Mater. Chem. C* **2021**, *9*, 13972.
[251] X. Liu, Z. Zhang, C. Wang, C. Zhang, S. Liang, H. Fang, B. Wang, Z. Tang, C. Xiao, W. Li, *Angew. Chem. Int. Ed.* **2024**, *63*, e202316039.
[252] S. Guan, Y. Li, C. Xu, N. Yin, C. Xu, C. Wang, M. Wang, Y. Xu, Q. Chen, D. Wang, L. Zuo, H. Chen, *Adv. Mater.* **2024**, *36*, 2400342.
[253] R. Po, A. Bernardi, A. Calabrese, C. Carbonera, G. Corso, A. Pellegrino, *Energy Environ. Sci.* **2014**, *7*, 925.
[254] T. P. Osedach, T. L. Andrew, V. Bulovid, *Energy Environ. Sci.* **2013**, *6*, 711.
[255] X. Liu, Y. Wei, X. Zhang, L. Qin, Z. Wei, H. Huang, *Sci. China Chem.* **2021**, *64*, 228.
[256] Z. P. Yu, Z. X. Liu, F. X. Chen, R. Qin, T. K. Lau, J. L. Yin, X. Kong, X. Lu, M. Shi, C. Z. Li, H. Chen, *Nat. Commun.* **2019**, *10*, 2152.
[257] C. Sun, F. Pan, H. Bin, J. Zhang, L. Xue, B. Qiu, Z. Wei, Z. G. Zhang, Y. Li, *Nat. Commun.* **2018**, *9*, 743.
[258] S. Zhang, Y. Qin, J. Zhu, J. Hou, *Adv. Mater.* **2018**, *30*, 1800868.
[259] F. Deschler, A. De Sio, E. von Hauff, P. Kutka, T. Sauermann, H. J. Egelhaaf, J. Hauch, E. Da Como, *Adv. Funct. Mater.* **2012**, *22*, 1461.
[260] B. C. Thompson, J. M. J. Fréchet, *Angew. Chem. Int. Ed.* **2008**, *47*, 58.
[261] C. J. Schaffer, C. M. Palumbiny, M. A. Niedermeier, C. Jendrzejewski, G. Santoro, S. V. Roth, P. Müller-Buschbaum, *Adv. Mater.* **2013**, *25*, 6760.
[262] L. T. Nchinda, Z. Genene, W. Mammo, N. A. Tegegne, T. P. J. Krüger, *New J. Chem.* **2024**, *48*, 10201.
[263] T. Heumueller, W. R. Mateker, I. T. Sachs-Quintana, K. Vandewal, J. A. Bartelt, T. M. Burke, T. Ameri, C. J. Brabec, M. D. McGehee, *Energy Environ. Sci.* **2014**, *7*, 2974.
[264] M. B. Upama, M. Wright, M. A. Mahmud, N. K. Elumalai, A. Mahboubi Soufiani, D. Wang, C. Xu, A. Uddin, *Nanoscale* **2017**, *9*, 18788.
[265] B. Carsten, F. He, H. J. Son, T. Xu, L. Yu, *Chem. Rev.* **2011**, *111*, 1493.
[266] L. Zuo, S. B. Jo, Y. Li, Y. Meng, R. J. Stoddard, Y. Liu, F. Lin, X. Shi, F. Liu, H. W. Hillhouse, D. S. Ginger, H. Chen, A. K. Jen, *Nat Nanotechnol.* **2022**, *17*, 53.
[267] I. Fraga Domínguez, A. Distler, L. Luer, *Adv. Energy Mater.* **2017**, *7*, 1601320.
[268] J. Roncali, *Adv. Energy Mater.* **2011**, *1*, 147.
[269] L. Zuo, S. B. Jo, X. Shi, F. Lin, A. Jen, *Chin. J. Chem.* **2024**, *42*, 252.
[270] Y. He, T. Heumüller, W. Lai, G. Feng, A. Classen, X. Du, C. Liu, W. Li, N. Li, C. J. Brabec, *Adv. Energy Mater.* **2019**, *9*, 1900409.
[271] T. L. Nguyen, T. H. Lee, B. Gautam, S. Y. Park, K. Gundogdu, J. Y. Kim, H. Y. Woo, *Adv. Funct. Mater.* **2017**, *27*, 1702474.

Newayemedhin A. Tegegne is an Associate Professor of Physics at the Physics Department of Addis Ababa University, Ethiopia. She earned her Ph.D. in 2018 from the Laser Research Institute at Stellenbosch University, South Africa, specializing in femtosecond transient-absorption spectroscopy. Following her doctoral studies, she completed a postdoctoral fellowship at the University of Pretoria's Department of Physics. Dr. Tegegne leads a research group focused on understanding efficiency and stability factors in organic solar cells, investigating structure-property relationships, surface modifications of transport layers using self-assembled monolayers, and their associated photophysics.

Leonato T. Nchinda is a Ph.D. candidate at the University of Pretoria, South Africa, focusing on the stability and photophysics of organic solar cell active layers based on multicomponent polymer materials. He holds a B.Sc. and M.Sc. in Physics from the University of Buea, Cameroon. His research interests are centered around the utilization of spectroscopic techniques such as femtosecond transient-absorption spectroscopy in conjunction with morphological characterization techniques to study degradation mechanisms and charge dynamics in organic solar cells. He is dedicated to advancing renewable energy technologies and addressing global energy challenges.

© 2024 The Author(s). Advanced Optical Materials published by Wiley-VCH GmbH

Tjaart P. J. Krüger is an Associate Professor in the Department of Physics at the University of Pretoria. He completed a Ph.D. in 2011 from the Vrije Universiteit Amsterdam. His research interests include developing and using advanced laser spectroscopy techniques, complemented by theoretical and computational approaches, to resolve the molecular details of energy transfer and regulation in various natural light-harvesting complexes and to apply the underlying design principles to organic solar cells. He is a former executive committee member of the South African Young Academy of Science and a current councilor of the International Union for Pure and Applied Biophysics.

© 2024 The Author(s). Advanced Optical Materials published by Wiley-VCH GmbH